2015

Characterization of Highly Concentrated Elastin-Like Polypeptide Solutions: Rheometric Properties and Phase Separation Analysis

Kevin Michael Otto
Cleveland State University

CHARACTERIZATION OF HIGHLY CONCENTRATED ELASTIN-LIKE POLYPEPTIDE SOLUTIONS: RHEOMETRIC PROPERTIES AND PHASE SEPARATION ANALYSIS

KEVIN M. OTTO

Bachelor of Science in Chemical Engineering

Cleveland State University

May 2013

Submitted in partial fulfillment of requirements for the degree

MASTER OF SCIENCE IN CHEMICAL ENGINEERING

at the

CLEVELAND STATE UNIVERSITY

MAY 2015

We hereby approve this thesis for

Kevin M. Otto

Candidate for the Master of Science in Chemical Engineering degree for the

Department of Chemical and Biomedical Engineering

and the CEVELAND STATE UNIVERSITY

College of Graduate Studies by

_____

Thesis Chairperson, Dr. Nolan B. Holland
Department of Chemical and Biomedical Engineering
Cleveland State University

_____

Date

_____

Thesis Committee Member, Dr. Dhananjai B. Shah
Department of Chemical and Biomedical Engineering
Cleveland State University

_____

Date

_____

Thesis Committee Member, Dr. Christopher Wirth
Department of Chemical and Biomedical Engineering
Cleveland State University

_____

Date

Date of Defense: 4/30/2015

ACKNOWLEDGMENTS

First and foremost, I would like to thank my research advisor, Dr. Nolan B. Holland, for the opportunity he provided me to be part of his team and join his laboratory. He provided me with help, support, and guidance during my studies which is immensely appreciated. He helped me to further understand many concepts and ideas as well as expanded my knowledge to new areas. It has been a wonderful and fulfilling experience for me to work in his laboratory under his guidance. I must also express my thanks to my thesis defense committee members Dr. Dhananjai B. Shah and Dr. Christopher Wirth. Their time in being on my committee and reviewing my thesis is much appreciated.

I would like to also thank all the faculty and staff members of the Chemical and Biomedical Engineering Department at Cleveland State University. They provided a wonderful atmosphere to be around and had very friendly, happy attitudes that made it a pleasant place to conduct my studies. A special thank you goes out to Becky Laird and Darlene Montgomery for their continuous support and help throughout my time at Cleveland State University. They both were always very willing to answer any questions I had and were always friendly.

My colleagues who also worked in Dr. Holland's laboratory were fantastic. They were continuously supportive and willing to help. Throughout my time in this laboratory they became more than colleagues, but friends. Thank you to James Cole for his patience, and his willingness to teach me methods and useful information regarding my research.

I must also thank my incredible family especially my parents, James and Charlene Otto. They have been absolutely nothing but supportive and encouraging throughout all

of my time at Cleveland State University. Without the help of my wonderful parents there is no way I would be where I am today. I would also like to thank my amazing fiancée, Annie Doyle for her never ending love, support, and understanding throughout the completion of my schooling.

CHARACTERIZATION OF HIGHLY CONCENTRATED ELASTIN-LIKE POLYPEPTIDE SOLUTIONS:

RHEOMETRIC PROPERTIES AND PHASE SEPARATION ANALYSIS

KEVIN OTTO

ABSTRACT

Elastin-like polypeptides (ELPs) are environmentally responsive biopolymers. These protein based polymers are specific in that they exhibit phase separation in response to a number of stimuli. Some of these stimuli include temperature, light, and pH. There are a large number of factors to consider when designing ELP constructs that allow for control of the transitioning behavior, some of which include amino acid sequences, protein concentration, salt concentration, and the polymer chain length.

Elastin-like polypeptides are soluble in water at low temperatures, however, upon an increase in temperature, the proteins become insoluble in water and phase separate. This point of temperature triggered phase transitioning shows lower critical solution temperature (LCST) behavior and is referred to as the inverse transition temperature (T_t). The transition is completely reversible and the ELPs will return back into solution upon decreasing temperature below the T_t.

The linear elastin-like polypeptide $(GVGVP)_{40}$ and the trimerized $(GVGVP)_{40}$-foldon were expressed in a bacterial system using *Escherichia coli* (*E. coli*). Exploiting ELP temperature triggered transitioning to an insoluble state, highly concentrated protein solutions were formed for each sample.

In this study, various rheometric experiments were conducted on $(GVGVP)_{40}$ and $(GVGVP)_{40}$-foldon. The storage, G', and loss, G'', dynamic moduli were determined to characterize the viscoelastic behavior of highly concentrated ELP solutions. Shear viscosities as functions of time, temperature, and concentration were determined. As well, various other rheological properties were determined and used to help better understand and characterize these highly concentrated ELP solutions. The ELPs studied showed shear thinning characteristics along with more viscous compared to elastic behaviors at all angular frequencies. A power law model was fit to relate the viscosity of the solutions to the protein concentration.

Starting at high concentrations then diluting stepwise the transition temperatures of $(GVGVP)_{40}$ were determined and characterized using UV-Visible spectrophotometry. The purpose was to obtain a better understanding of the phase diagram for the transitioning from single phase to multiphase systems. Multiple methods for analysis of transition temperature are proposed and transition temperatures were calculated based on each method, resulting in multiple different phase diagrams. A model was fit to the phase diagrams that predict the transition temperature as a function of protein concentration at low concentrations.

TABLE OF CONTENTS

LIST OF FIGURES

LIST OF TABLES

LIST OF IMPORTANT EQUATIONS

RHEOLOGY NOMENCLATURE

Symbol	Description
γ	Oscillatory strain
γ_o	Applied oscillatory strain
σ	Oscillatory stress
σ_o	Applied oscillatory stress
f	Frequency
ω	Angular frequency
t	Time
δ	Phase angle
σ'	In-phase stress
σ''	Out-of-phase stress
${\sigma_o}'$	In-phase applied stress
${\sigma_o}''$	Out-of-phase applied stress
G'	Storage modulus
G''	Loss modulus
G^*	Complex modulus
η'	Dynamic (in-phase) viscosity
η''	Out-of-phase viscosity
η^*	Complex viscosity

CHAPTER I

INTRODUCTION AND BACKGROUND

1.1 Introduction of Elastin-like Polypeptides

Elastin-like polypeptides (ELPs) are environmentally responsive biopolymers. These protein based polymers have specific amino acid sequences which determine their biological activity and properties. ELPs seem generally attractive for many biological applications due to the synthesis using genetic encoding, which provides control over chain length and amino acid sequences. Using molecular biology along with recombinant DNA technologies, vast arrays of materials involving specific amino acid sequencing have been created [1]. When compared to synthetic polymer synthesis, protein based polymers offer many potential advantages due to the structural control and complexity of the systems [2].

Polypeptides consist of multiple amino acids bonded to one another covalently [5]. When amino acids covalently bond to one another, the peptide bond formed occurs when the carboxyl group of one molecule reacts with the amine group of another molecule (*Figure 1.1*). This chemical bonding results in the production of water along with the polypeptide. All peptide chains always have a carboxyl group at one end of the chain which is referred to as the C-terminus. At the opposing end of the chain, there exists an amino group which is termed the N-terminus. Amino acids are often represented by a single letter abbreviation with the protein sequence written in order from the N-terminus to the C-terminus.

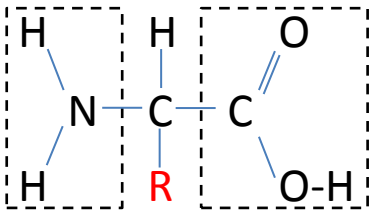

Figure 1.1: General structure of an amino acid. The left box represents an amino group while the right box represents a carboxyl group. The "R" represents the side chains that determine each individual amino acid.

This basic structure of elastin-like polypeptides is a repeating amino acid sequence found within the mammalian protein elastin [1]. The mammalian protein elastin is a polymeric protein which imparts elastic recoil and extensibility to large blood vessels, lung parenchyma, and skin [3]. One of the more common embodiments of the pentapeptide sequence is glycine-valine-glycine-valine-proline or, (GVGVP) (a repeated sequence found within the amino acid sequence of elastin). Aside from the construct GVGVP, ELPs can be modified based on repeats of the pentapeptide $(G\alpha G\beta P)_n$. Here, α

can be any of the 20 naturally occurring amino acids while β can also be any of the naturally occurring amino acids excluding proline (P) [4]. The physical, chemical, and especially biological properties exerted by ELPs are ideal for some important biomedical applications which will be discussed further. Thus, there is much interest in understanding and utilizing these polymers and they are continuously the subject of new studies and discoveries.

Elastin-like polypeptides exhibit a reversible phase transitional behavior related to changes in temperature. This phase transitioning behavior is referred to as an inverse transition temperature or, T_t [6]. There are a number of various environmental conditions as well as structural effects that affect ELPs T_t. Below the T_t, the polymer chains in solution exhibit a free random coil configuration. Upon heating, above the T_t, the ELP phase separates and the chains are believed to undergo hydrophobic folding and assembling. In this state the polymer chains form a regular, more stabilized and organized structure. Previous studies show the result of this chain folding above the ELPs transition temperatures is a phase separated sample containing approximately 37% protein and 63% water [7].

In comparison to conventional polymers, ELPs offer many potential benefits and advantages. One of the most important of these advantages is the transitioning behavior that is exhibited by ELPs. This particular property allows for numerous applications. Another valuable asset of elastin-like polypeptides is their ability to be synthesized by recombinant DNA techniques and chemical methods allowing for precise control of single constructs [8].

1.2 Applications of Elastin-like Polypeptides

Elastin-like polypeptides have many valuable applications. Currently, ELPs are being used in biomedical applications due to the ability to precisely control the molecular weight, chain length, amino acid sequences, and their biocompatibility [9]. Some of the more common applications include drug delivery, tissue engineering, and hydrogels.

1.2.1 Elastin-like Polypeptides as Drug Delivery Systems

Stimulus-responsive biomaterials are a promising resource with applications in controlled drug delivery. Elastin-like polypeptides have had continuing growing interests for utilization in biomedical applications. This is due their biocompatibility, biodegradability, they can be designed to be non-toxic, and they exhibit good pharmacokinetics [10, 11, 12]. Given that ELPs exhibit this biocompatibility, they are suitable for local and systematic administrations, as they induce minimal inflammatory and immune effects in animal models [13, 14] and can be administered to humans without eliciting an adverse immune response [15].

The genetically encoded design of ELPs permits exact control over the sequence of the ELP. This can be exploited to precisely specify the location at which biological drug-peptide or protein is fused to an ELP, or the location at which a reactive residue is placed for covalent conjugation of the ELP with small molecule drugs [16]. The molecular weight influences important biological parameters such as circulation clearance allowing for improved prediction of ELP behavior *in vivo*, as compared to alternative polydisperse materials [16]. The biological compositions of elastin-like

polypeptides also ensure their biodegradation which allows for their safe breakdown into peptides and amino acids which can then be easily cleared from the body.

1.2.2 Elastin-like Polypeptides in Tissue Engineering

Elastin-like polypeptides can be utilized in tissue engineering applications, not only due to their biocompatible, biodegradable, and non-immunogenic properties, but also because their amino acid sequence and molecular weight can be precisely controlled at the genetic or synthetic level, thus allowing exquisite control over the final proteins functionality [18]. Biomaterials used in tissue engineering applications must have the ability to fill and assume the shape of a replacement tissue, void or defect, support necessary cellular processes needed for regeneration of tissue that will function like native tissue, enable efficient nutrient and waste exchange to support those cells, supply necessary physical properties required for a given tissue, and remain fixed within the target area for a specific period of time [17].

These goals have been targeted by various naturally occurring as well as synthetic polymers which take on a number of different forms of which include gels, foams, felts, and meshes [18]. One common obstacle when engineering and designing these optimal biomaterials (with varying functionalities) is the challenge of meeting many, often competing, design goals with any strategy used. An example of this would be a synthetic polymer being biocompatible however lacking cues for cell attachment and tissue growth. This ultimately leads to the need for modification of polymer sequence and other various factors.

To recapitulate, there are a few main reasons for the attraction and interests of elastin-like polypeptides used in tissue engineering. Firstly, ELPs can be genetically encoded. Their synthesis from a synthetic gene in a heterologous host (i.e. bacteria) provides complete control over amino acid sequences and molecular weight in which both are not easily controlled in many synthetic polymers. Secondly, ELPs have to ability to be readily purified from *E. coli* by making use of their inverse transition temperature phase transitioning without the need for chromatography, making for less intensive scale up purifications [19]. Also, ELPs can be designed and engineered to approach the viscoelastic properties of native elastin through cross-liking and other techniques. Lastly, ELPs can be biocompatible, biodegradable, and also non-immunogenic [13].

1.2.3 Elastin-like Polypeptides as Hydrogels

Hydrogels are three-dimensional polymer networks that have the ability to swell and do not dissolve in water. These structures have the capability to hold copious amounts of water exceeding 90 weight percent. Using various techniques, ELPs have the ability to be cross-linked including various chemical and physical forms. When producing cross-links in ELPs it is important to consider the methods and materials used in doing so. Many efforts have been made to insure biocompatibility and biodegradation. In the last several decades hydrogels have been used as parts of surgical sutures, soft contact lenses, drug delivery systems, and artificial organs [20]. ELP hydrogels seem to be particularly promising for musculoskeletal and cardiovascular applications due to their peptide sequences being native to smooth and skeletal muscle, ligaments, and other musculoskeletal tissues [21].

1.3 Temperature Dependence of Elastin-like Polypeptides

Elastin-like polypeptides undergo a reversible phase transition referred to as an inverse transition temperature (T_t) which shows lower critical solution temperature (LCST) behavior. The T_t of a polymer is represented by a specific temperature and polymer concentration in which below these conditions the solution is miscible and exhibits a single phase. As the temperature is increased to that greater than the T_t, the solution exhibits phase separation.

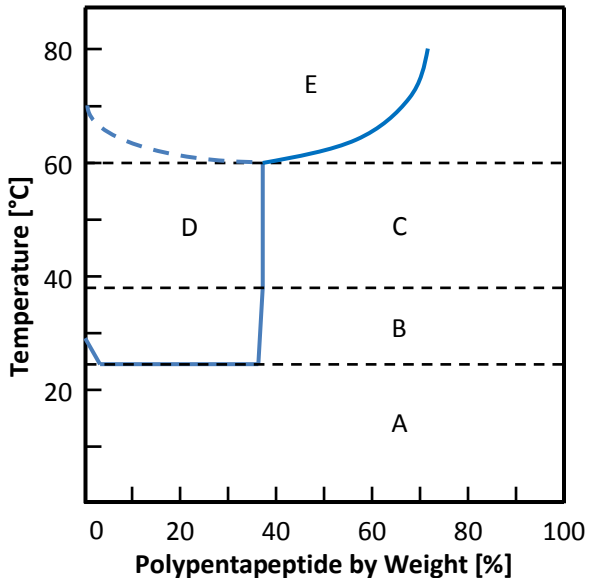

Figure 1.2: Phase diagram depicting a polypentapeptide-water system (adapted from reference [22]). Region *A*: Single phase; miscible in all portions. *B*: Structural transition region. *C*: Single phase; drying coacervate. *D*: Two phase; equilibrium solution and coacervate. *E*: Heat denaturation.

In *Figure 1.2* the phase diagram is demonstrated for a polypentapeptide-water system. On the x-axis the polypentapeptide weight percent is shown while on the y-axis the temperature in degrees Celsius is given. In region *A* of the diagram, from

approximately 0-25 °C the polypentapeptide and water are completely miscible as a single phase regardless of the polymers weight percent. As the temperature is increased to that exceeding 25 °C (the LCST), at protein concentrations of approximately 0-37% protein, phase separation occurs (region *D*). If looking at a temperature of 35 °C for example, at this point on the phase diagram there will exist two phases. In one of the phases there will exist a protein poor equilibrium solution and a protein rich solution containing nearly 40% protein with remainder water. Upon exceeding 60 °C, there is a denaturation of the polymer in solution. When speaking particularly of ELP solutions, the transition from one to two phases can be seen visually by an onset of turbidity leading to aggregation (*Figure 2.1*).

1.4 Factors Effecting Inverse Transition Temperature, Tt

The ability to manipulate and alter the transition temperatures for elastin-like polypeptides can prove largely useful. There are a number of factors that contribute to the inverse transition temperature of elastin-like polypeptides. Some of the more significant factors include pH, salt concentration, protein concentration, amino acid composition, and chain length [23, 24].

1.4.1 Effect of pH on Elastin-like Polypeptide T_t

The transition temperature of elastin-like polypeptides is pH responsive due to the dependence on the mean polarity of the polymer [25]. A study was conducted which described the phase behavior of pH-responsive ELPs acidic and basic residues [26]. In this study, the authors designed pH-responsive ELPs, in which the acidic ELPs are charged above their $pK_{a,}$ resulting in a high T_t. When the pH is less than the ELPs pK_a,

the acidic residues become protonated and neutral thus leading to a decrease in T_t. Additionally, when the ELPs are basic at lower pH, they are soluble and upon pH exceeding $pK_{a,}$ they neutralize and in response a lower T_t is exhibited.

1.4.2 Effect of Salt Concentration on Elastin-like Polypeptide T_t

There have been a multitude of studies conducted regarding the effects of varying salt concentrations in ELP solutions. The effect of salt concentration on the transition temperature of elastin-like polypeptides has been well defined as a linear relationship [4]. As the concentration of sodium chloride is increased the ELP transition temperature decreases. For this reason, the addition of NaCl to ELP solutions is often used as an easy means for decreasing the transition temperature. Investigations were completed by Urry *et al*. which examined the effects of NaCl on the exothermic and endothermic components of the lower critical solution temperature [27, 28]. This study concluded that an increase in NaCl concentration has a significant effect on, and decreases the transition temperature. This study also concluded that the addition of NaCl increased the transition enthalpy of the system. With increasing salt concentrations, exothermic behavior which can be described by folding and association and endothermic behavior is described as the disruption of ordered water structures both increased with increasing salt concentrations. This led the authors to determine that the effect of NaCl concentration cause increase in organization of ELPs in the folded state and improved structure of hydrophobic hydration surrounding chains.

When a comparison was done on a linear ELP, $(GVGVP)_{40}$ and a trimerized ELP, $(GVGVP)_{40}$-foldon of varying salt concentrations it was determined that the linear and

trimerized proteins transition temperatures had nearly identical linear slopes (*Figure 1.3*) in relation to decreasing T_t [4]. What this study concluded is that the salt concentration effects on T_t are completely independent of the proteins geometries as well as molecular weights.

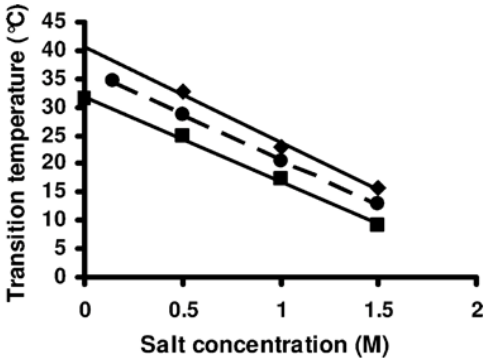

Figure 1.3: Effects of salt concentration on transition temperatures for $(GVGVP)_{40}$ (diamonds), $(GVGVP)_{40}$-foldon (circles), and $(GVGVP)_{120}$ (squares) (Reprinted with permission from reference [4]. Copyright 2010 American Chemical Society).

A study was completed which investigated the resulting transition temperature with regards to NaCl addition together with addition of additives including SDS on the ELP, $(VPGIG)_{40}$, in aqueous solutions [29]. As expected, with an increase in salt concentration came a linear decrease in transition temperature. The addition of SDS at various concentrations proved to have a significant effect on the behavior of the transition temperature. With the addition of SDS, exceeding values of the critical micelle constant of SDS, caused a lowering of transition temperature. On the other hand, when values of SDS were less than the critical micelle constant, a gradual increase in T_t was observed. In order to describe these results the authors explain how salts such as NaCl have lower lyotropic numbers which induce the globular state of polymers [30]. The salts strengthen

the hydrophobic interactions allowing for the ELPs to hydrophobically fold and assemble therefore lowering the lower critical solution temperature [29].

1.4.3 Effect of Elastin-like Polypeptide Chain Length on T_t

Elastin-like polypeptide chain lengths have been shown to play a large roll in shifting of transition temperatures. Meyer and Chilkoti describe multivariate equations which examine the transition temperature as functions of chain length, concentrations, and various constraints [31]. Their studies concluded that concentration of ELP and chain length have a more significant impact on ELP transition temperatures that are low in peptide concentration and chain length. It has been determined by a number of studies that the shorter an ELPs chain length, the higher the transition temperature exhibited when compared to that of larger chain lengths [31].

Rodriguez-Cabello and Reguera studied the effects of molecular weight (i.e. chain length) and determined there were a decrease in T_t along with an increase in transition enthalpy with increasing ELP molecular weight [25]. This behavior exhibited an asymptotic effect. At lower molecular weights the increase was quite significant however; at higher molecular weights the effects were much less significant.

1.4.4 Effect of Elastin-like Polypeptide Concentration on T_t

Elastin-like polypeptide concentration has been shown to have a significant effect on the altering of transition temperature. The effects of ELP concentrations were described in two ways [32]. Firstly, at low ELP concentrations the transition temperature increased because the interchain cooperativity necessary for correct ELP folding does not take place as efficiently in dilute peptide concentrations. What was determined from this

study was a concentration limit was exhibited in which the effect of increasing ELP concentration no longer changed the T_t. Secondly, at high ELP concentrations there was an inability for the ELP to fold completely causing an increase in T_t.

1.5 Structural Changes of Elastin-like Polypeptides

Early studies focused on proving the existence of structural intermediates and starting in the1980's research on protein folding intermediates increased significantly [33]. Phase transitioning of ELPs have been proven to exhibit conformational changes using techniques that are discussed further section *1.6* [6, 34, 35]. The behavior and functionality of ELPs are derived from the amino acid sequence, aggregated structure, and protein folding. The basic model for the transitioning of ELPs from the relaxed elastomeric random coil conformation to aggregates was proposed by Urry (*Figure 1.4*).

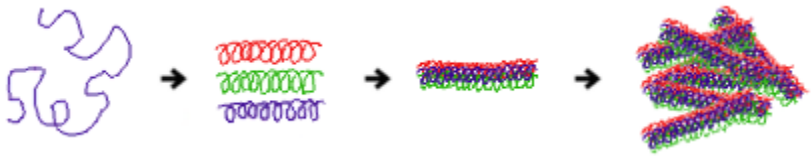

A. **B.** **C.** **D.**

Figure 1.4: Transition of a random coil chain as a function of increasing temperature to temperatures exceeding the transition temperature (adapted from reference [4]).
A: Random coil. *B*: β-spiral. *C*: Triple Helix. *D*: Aggregate.

Studies have shown the existence of β-structured spirals of ELPs through computer simulations in which rigid conformational states where observed at lower temperatures while, on the other hand, a more flexible state was shown at higher temperatures [47]. ELPs seem to show typical elastin-like conformational behavior. Upon

increase in ELP temperature, a decrease in random coil and an increase in β-spiral characteristics are observed.

Under appropriate conditions (i.e. salt, pH, concentration) certain constructs of ELPs have the ability to form micelles. Micelles nanoparticles are surfactant based particles consisting of hydrophilic head groups and hydrophobic tail groups. At low temperatures ELPs are soluble in water however, at temperatures exceeding the transition temperatures they become insoluble. Ghoorchian *et al*. performed studies of ELP constructs containing a charged trimer forming domain. This domain connects three ELP monomer chains together as well as adds a hydrophilic head group. Upon exceeding transition temperatures this trimerized system behaves as a surfactant and forms micelles. These small aggregates contain hydrophobic head groups surrounding the hydrophilic tail core (*Figure 1.5*). The variation of salt concentration plays an important role and dictates the size and type of aggregation that occurs in the creation of micelles.

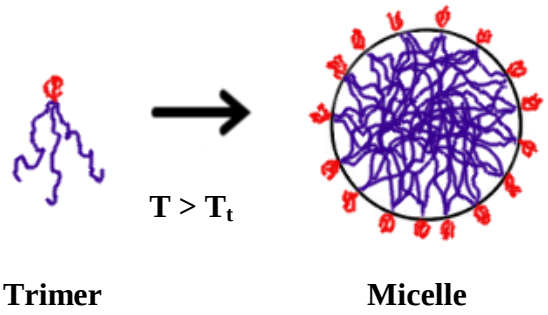

Figure 1.5: Transition from random coil timer to micelle with increasing temperature.

The key effect of the addition of salt into solutions is the moderation of electrostatic interactions between charged species. Salt can also modify hydrophobic interactions. This manipulation of hydrophobic interactions can be observed by the dependence of salt on the transition temperature of ELPs [4].

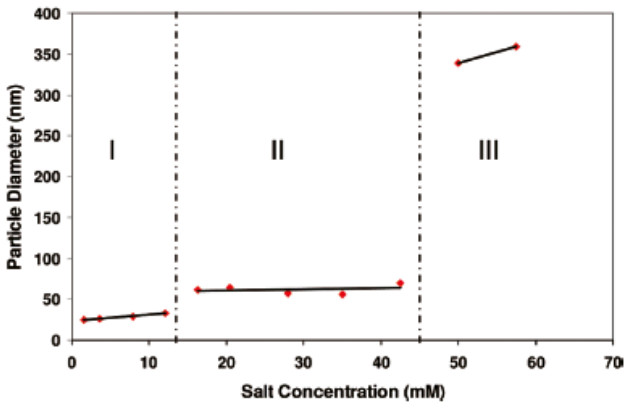

Figure 1.6: Particle diameter with respect to salt concentration for $(GVGVP)_{40}$-foldon using dynamic light scattering (DLS). A 10 μM polypeptide solution was studied at 50 °C which is greater than the T_t (Reprinted with permission from reference [4]. Copyright 2010 American Chemical Society).

Three regions were observed in the study by Ghoorchian *et al*. from *Figure 1.6* above [4]. In region I, for salt concentrations less than 15 mM, the particles are all under 30 nm and appear to linearly increase with salt concentration. For region II, for salt concentrations of 15-45 mM the size of the aggregates are approximately constant at around 60-65 nm in diameter. In region III, greater than 45 mM, the aggregates are much larger at around 300 nm. Approaching region III, visual turbidity was observed from the solution.

1.6 Characterization

There are a number of techniques used in the characterization of peptides and proteins. The methods used in characterizing elastin-like polypeptides are the commonly used methods in general for protein characterization. Some common methods of characterization are discussed.

To measure the transition temperatures, UV-visible spectrophotometry and differential scanning calorimetery (DSC) are often used [36]. To characterize purity of proteins often electrophoresis-based methods such as SDS-PAGE are utilized. For molecular weight characterization some methods include SDS-PAGE and mass spectrometry (MS) methods, such as matrix-assisted laser desorption ionization (MALDI MS) and electrospray mass spectrometry (ESI MS) [2]. For surface behavior and binding of peptide based biomaterials, surface plasmon resonance spectroscopy (SPR) may be used [48].

The structural properties of elastin-like polypeptides play an important role in their applications and their designs. In order to determine such properties (i.e. particle sizing, etc.) such techniques include dynamic light scattering (DLS). To characterize the protein folding that is exhibited by ELPs methods such as differential scanning calorimetry (DSC) and circular dichroism spectrometry (CD) are used [38, 39].

Rheology, the study of flow and deformation of matter, is a multidisciplinary science that allows for the measurement of force and deformation of time dependent materials. This science is used in characterizing the interrelations between flow, deformation, and time. Rheology encompasses many very important engineering areas of

which some of the more predominant include polymers, biotechnology, paints, adhesives, lubricants, and surfactants. There are many situations in which the deformation or the flow of matter (which depends on the rheological characteristics of the materials involved) determines the performance of a product, the effectiveness of a service, and the rate of a manufacturing process [42].

One of the main focuses of this study is to understand the mechanical properties of ELPs, in particular viscoelasticity. Viscoelasticity of a material is a property exhibiting both viscous and elastic characteristics during deformation. To understand this and other mechanical properties of elastin-like polypeptides various rheological tests are performed.

Various rheometric experiments were conducted on $(GVGVP)_{40}$ and $(GVGVP)_{40}$-foldon. The proteins storage and loss moduli were determined in order to analyze and characterize viscoelastic behaviors. Storage modulus, G', is a measure of a materials ability to store energy and is known as the elastic response. Loss modulus, G'', is a measure of a materials ability to dissipate energy, also known as viscous behavior. Oscillatory shear experiments (sinusoidal oscillations) are performed in which the sample is exposed to a sinusoidal strain, γ, at a fixed angular frequency, ω, and will respond with a sinusoidal stress, σ. The resulting stress will often be shifted by a phase angle, denoted δ. The following are representative of the basic equations used in calculation of the data collected throughout the course of this study during the experiments on the rheometer.

Equation 1.1 displays the equation for applied *oscillatory strain* and *Equation 1.2* demonstrates the equation for sinusoidal *stress response* [41].

$$\gamma = \gamma_o \sin(\omega t) \qquad \textit{Eqn. 1.1}$$

$$\sigma = \sigma_o \sin(\omega t + \delta) \qquad \textit{Eqn. 1.2}$$

Such data is analyzed by decomposing the stress wave into two waves of the same frequency, one in-phase with the strain wave *(*sin*(ωt))* and one 90° out-of-phase with the strain wave *(*cos*(ωt))* [42]. Therefore,

$$\sigma = \sigma' + \sigma'' = \sigma_o' \sin(\omega t) + \sigma_o'' \cos(\omega t) \qquad \textit{Eqn. 1.3}$$

Using trigonometry and *Equation 1.3*,

$$tan\delta = \frac{\sigma_o''}{\sigma_o'} \qquad \textit{Eqn. 1.4}$$

This suggests two dynamic moduli *G'* and *G"*,

$$G' = \frac{\sigma_o'}{\gamma_o} \qquad \textit{Eqn. 1.5}$$

G', the in-phase elastic component termed *storage modulus*, also,

$$G'' = \frac{\sigma_o''}{\gamma_o} \qquad \textit{Eqn. 1.6}$$

G", the out-of-phase viscous component termed *loss modulus*.

Using *Equation 1.4* from above in combination with *Equations 1.5 and 1.6* we can write,

$$tan\delta = \frac{G''}{G'} \qquad \textit{Eqn. 1.7}$$

Equation 1.7 is known as the *damping factor* or *loss tangent*. The strain, γ, can be represented as the imaginary part of a complex number $\gamma_o e^{i\omega t}$ and likewise $\sigma' = Im\{\sigma_o e^{i\omega t}\}$ and $\sigma'' = Re\{\sigma_o e^{i\omega t}\}$ [42]. Thus, the variable *G** can be defined as,

$$\sigma_o = |G^*|\gamma_0 \qquad \textit{Eqn. 1.8}$$

Here, *G** is the *complex number*, or, *complex modulus* with *G'* as the real portion and *G''* as the imaginary part. Therefore, *Equation 1.9* may be written,

$$G^* = G' + iG'' \qquad \textit{Eqn. 1.9}$$

Therefore, *Equation 1.3* may be rewritten,

$$\sigma = G'\gamma_o \sin(\omega t) + G''\gamma_o \cos(\omega t) \qquad \textit{Eqn. 1.10}$$

From the magnitudes of the viscous stress to the strain rate, a *dynamic viscosity* may be defined as follows in *Equation 1.11* [42],

$$\eta' = \frac{\sigma_o''}{\dot{\gamma}_o} = \frac{G''}{\omega} \qquad \textit{Eqn. 1.11}$$

An elastic portion of the complex viscosity may also be defined as follows in *Equation 1.12*,

$$\eta'' = \frac{\sigma_o'}{\dot{\gamma}_o} = \frac{G'}{\omega} \qquad \textit{Eqn. 1.12}$$

Thus, a magnitude of *complex viscosity* (*Equation 1.13*) may be defined [42],

$$|\eta^*| = (\eta'^2 + \eta''^2)^{\frac{1}{2}} = \left[\left(\frac{G''}{\omega}\right)^2 + \left(\frac{G'}{\omega}\right)^2\right]^{\frac{1}{2}} = \frac{1}{\omega}|G^*| \qquad \textit{Eqn. 1.13}$$

For a purely elastic material, the stress and strain are perfectly in phase with one another. The phase angle, δ, is equal to 0°. It can be said that the material will react immediately to an applied stress or strain. For a material that is purely viscous, the stress and strain are out of phase thus there will be a lag in material response. The phase angle here is equivalent to $\frac{\pi}{2}$ or 90°. When a material exhibits both elastic and viscous characteristics (i.e. viscoelastic material) the phase angle will be somewhere in-between 0 to $\frac{\pi}{2}$, or, 0° to 90° (*Figure 1.7*).

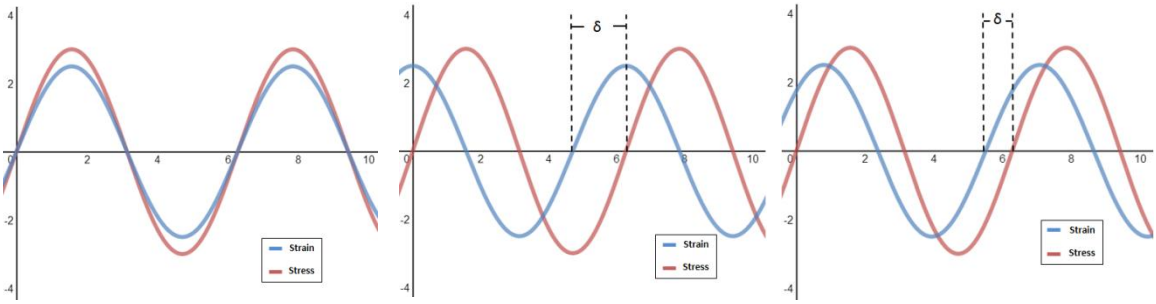

A. B. C.

Figure 1.7: Graphical representation of stress and strain waves of various material types with respect to time. *A*: example of a purely elastic material applied strain with resulting stress, $\delta = 0$. *B*: example of a purely viscous material applied strain with resulting stress, $\delta = \frac{\pi}{2}$. *C*: example of a viscoelastic materials applied strain with resulting stress, $0 < \delta < \frac{\pi}{2}$.

There are many geometries available for rheometers all having both advantages and disadvantages (*Figure 1.8*).

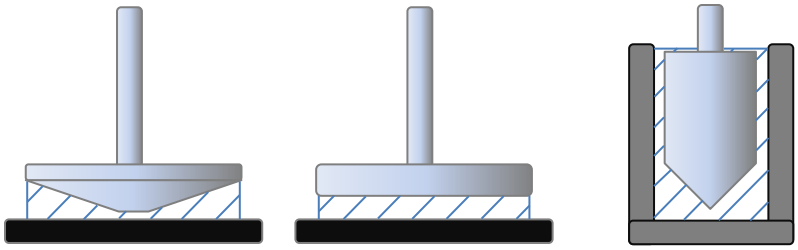

A. B. C.

Figure 1.8: Common rheometer geometries. *A*: Cone (1° to 5° angle) and Plate. *B*: Parallel Plates. *C*: Cup and Bob (Concentric Cylinders). The blue lines represent the area in which the sample occupies.

The cone and plate consists of a cone with an angle of 1° to 5° and a flat bottom platform. The parallel plates consist of a flat top plate with a flat bottom platform. The cup and bob consists of an inner cylinder with a conical bottom that rest within another cylinder of slightly larger diameter. Listed below in *Table 1.1* are some of the important advantages and disadvantages of the available geometries.

Geometry	Advantages	Disadvantages
Cone and Plate	-Uniform shear rate across cone -Small sample size required (~.8 ml) -Wide viscosity range	-High solvent evaporation -Large effects of loading
Parallel Plates	-Flexible gap height -Small sample size required (~1 ml)	-Shear rate dependency -High solvent evaporation -Large effects of loading
Cup and Bob	-Good for samples of low viscosity -Small impact of loading error -Small effects of evaporation	-Large sample size required (~15 ml) -High moment of inertia

Table 1.1: Advantages and disadvantages of common rheometer geometries.

CHAPTER II

MATERIALS AND METHODS

2.1 Overview

This section explains the methods and materials that were utilized in expression, purification, and characterization of the ELP proteins used through the course of this study. The two constructs expressed for this study were the linear polymer, $(GVGVP)_{40}$, and the trimerized $(GVGVP)_{40}$-foldon. Upon completion of expression and purification the concentrations of the proteins were measured and the samples were then ready for further analysis.

2.2 Expression and Purification of Elastin-like Polypeptides

The inverse transition temperatures experienced by these proteins were utilized in order to purify ELPs. The method used was inverse transition cycling (ITC) which is a

process of selective aggregation by heating the cell lysate and / or adding NaCl. ITC is both cost and time efficient because this purification method eliminates the need for chromatography. This method is laid out and described by Urry [43, 44]. The elastin-like polypeptides used in this study are presented below in *Table 2.1*.

ELP	Amino Acid Sequence	Molecular Weight (g/mole)
$(GVGVP)_{40}$	$MGH(GVGVP)_{40}GWP$	17,063
$(GVGVP)_{40}$-foldon	$MGH(GVGVP)_{40}GWPGYIP$ EAPRDGQAYVRKDGEWVLLSTFL	20,143

Table 2.1: Elastin-like polypeptides including amino acid sequences and molecular weights. Molecular weights were calculated based on the amino acid compositions.

2.2.1 Preparation of Media

To prepare the media the following were combined:

- 12 g of Peptone
- 24 g of Yeast Extract
- 12.5 g of Dipotassium Phosphate (K_2HPO_4)
- 2.3 g of Monopotassium Phosphate (KH_2PO_4)

These four ingredients were added into 1 liter of pure RO H_2O. Upon dissolving into the water the media was autoclaved for sterilization. After the media had cooled to room temperature 100 mg of the antibiotic ampicillin was added per liter of media.

2.2.2 Starter Cell Cultures and Expression

Cell cultures were prepared using samples of media taken from the previous step. Using culture tubes, 10 ml of media was added. To the tubes, cells of the desired

construct were transferred from glycerol frozen stocks. The culture tubes were then incubated overnight for approximately 12-16 hours at 37 °C, shaken at 300 RPM, and filtered air was pumped in to increase oxygen content. For each one liter of media prepared, 20 ml of culture was added.

Expression was initiated when the starter cultures were transferred into the media. The cell density was now monitored using a BioMate 3 UV-Visible spectrophotometer to see when there was a sufficient amount of cells to start induction. A sample of media was taken prior to the cultures being added to be used as a blank measurement for measuring the cell growth. When the cell density measurements OD_{600} reached approximately 0.8-1.0 the expression was ready to be induced. To induce, 240 mg of isopropyl-β-D-thiogalactopyronoside (IPTG) was added per liter of media. The solution was then incubated and shaken for 4-5 hours at 37 °C and 300 RPM. After induction was complete, the culture was centrifuged at 4 °C and 11,300 RCF for 15 minutes in the Beckman J2-21 centrifuge. The pellets were collected and kept at -20 °C for later purification while the supernatant was discarded.

2.2.3 Sonication and Purification

The frozen pellets were allowed to thaw to room temperature. Once the pellets were thawed, they were re-suspended by vortexing in 10 ml of RO H_2O. Upon full resuspension, 3 samples were combined in a conical 50 ml Falcon tube and placed on ice for 20 minutes. Next, the samples were sonicated using a Fisher Scientific 550 Sonic Dismembrator. For sonication, the samples were placed into an ice slurry and placed under the sonicator tip. The sonicator was set to program 4 which sonicates for eight, 10

second increments at an intensity setting of 4, with 20 seconds of rest between each. After sonication the samples were immediately placed back on ice to allow cooling.

To purify ELPs, inverse transition cycling (ITC) [43] was used. Since the ELPs are completely soluble below their T_t, the ELP protein was collected as the supernatant at cold temperatures (4 °C). On the other hand, the ELPs phase separate above the T_t thus the pellets were collected at high temperatures (40 °C).

The first step was to perform a cold centrifuge cycle at 4 °C for each individual sample that eventually will make up the final highly concentrated protein. To do this, the samples were taken off the ice after sonication and the contents were transferred into high-speed round bottom centrifuge tubes. They were then centrifuged at 4 °C and 27,000 RCF for approximately 25 minutes. After completion, the supernatants (containing the ELP) were immediately removed and placed into new centrifuge tubes. The supernatants were then placed into an incubator at high temperatures (above the known or expected T_t of the ELP) to begin transitioning the ELP from soluble to insoluble. After approximately 2 hours the supernatant was centrifuged in a warm cycle at 40 °C and 27,000 RCF for around 25 minutes. Upon completion of the cycle the samples are immediately decanted to allow as little as possible of the pellet (containing the ELP) to go back into solution and the supernatant was stored elsewhere. The pellets were then re-suspended in 5 ml of RO H_2O and placed on ice. After the samples had cooled, they were once again centrifuged at 4 °C and 27,000 RCF. The supernatant was removed and placed in the incubator. The pellets for each cycle from this point on will get smaller in size. The samples were then again centrifuged 40 °C and 27,000 RCF. The pellets were re-suspended and placed on ice. Finally, the samples were centrifuged at 4 °C and 27,000

RCF. The final supernatant was filtered and transferred to a 50 ml Falcon tube and purification is complete.

Step	Temperature (°C)	RCF (x g)	Time (min)
COLD I	4	27,000	25
Incubate	$>T_t$		120
WARM I	40	27,000	25
Re-suspend Pellet			
COLD II	4	27,000	20
Incubate	$>T_t$		120
WARM II	40	27,000	20
Re-suspend Pellet			
COLD III (Final)	4	27,000	15

Table 2.2: Purification ITC and re-suspension procedure.

2.3 Protein Concentration Measurements

To measure the concentration of the ELP protein in solution a procedure described by Gill and von Hippel [45] was used. This method uses the value of molar extinction coefficients. This method is preferred as it requires little amount of protein to determine concentration. To measure the concentrations the ELPs have to be in their denatured state which they will already be as they are in a denatured state at room temperature (below their T_t).

Concentrations of the ELP samples were determined using the absorbance at 280 nm collected using a BioMate 3 UV-Visible spectrophotometer. To measure the concentration first a blank was measured which is the solvent used (RO H_2O for this study). To a quartz cuvette, 950 µl of pure RO H_2O was added and the blank was measured on the UV-Visible spectrometer. After, 50 µl of the protein sample to be measured was added to the blank and mixed by means of vigorous pipetting. The absorbance was then measured and recorded.

From here the protein concentration was calculated. To do this the Beer-Lambert Law equation is used as follows:

$$c = \frac{A}{\varepsilon L} \qquad \textit{Eqn. 2.1}$$

Where c is ELP concentration, A is the measured absorbance at a wavelength of 280 nm, ε is the molar absorptivity which for the ELPs in this study are based on the tyrosine and tryptophan content of the peptides [4] (5,500 1/M·cm for GVGVP linear and 13,490 1/M·cm for GVGVP foldon), and L is the light path length.

2.4 SDS-PAGE Gel

Sodium dodecyl sulfate polyacrylamide gel electrophoresis (SDS-PAGE) is a technique that utilizes the ability of proteins to move within an electrical current, which is a function of the protein's molecular weights. The addition of SDS detergent removes secondary and tertiary protein structures and maintains the proteins as polypeptide chains. The SDS detergent coats the proteins (proportional to molecular weight) and the same negative electrical charge is applied across all the proteins [46].

Upon completion of purification, the final proteins were tested using SDS-PAGE to confirm purity. First, a clean gel cassette was loaded into the container which housed the Tris-glycine SDS buffer. The first lane was loaded with the ladder (molecular weight marker). In the remaining lanes, the final protein samples were loaded. For each sample, 5 µl of protein sample was combined with 10 µl of nuclease-free water and 5 µl of 4X sample buffer dye. The samples were then loaded using a pipette to their appropriate lanes. Now the lid was attached and the power was set to 100 V for approximately 1.5 hours. Following completion, the gel was carefully removed from the cassette and placed in RO H_2O for a few minutes to wash it. The gel was placed in blue gel stain and allowed to soak for at least a few hours. Once again the gel was washed and left in water for preservation. The gels accurately confirmed all samples purities that were used throughout the course of this study.

2.5 Preparing Coacervate

The coacervates (highly concentrated dense protein) that were used in this study consisted of around 40% protein with remainder buffer (which for this study was RO H_2O). The required sample size for the coacervates studied using rheology was a minimum of approximately 0.8 ml. In order to achieve such sample sizes multiple expressions and purifications are required. Once enough protein to obtain the minimum value of coacervate had been expressed, the individual samples were combined into one solution. From this point one uniform coacervate was formed.

In order to settle the coacervate the samples had to be raised in temperature. In doing so, the samples needed to exceed their T_t. As the protein approached its T_t it

transitioned from soluble to insoluble in solution. Thus, it was important that the protein be insoluble so it phase separated into a protein rich coacervate and a protein poor supernatant (*Figure 2.1*).

A. **B.** **C.** **D.**

Figure 2.1: Transition from soluble solution to insoluble phase separated solution. *A*: Protein solution at room temperature (single phase). *B*: Turbid solution transitioning from soluble to insoluble. *C*: Powder like mass of protein. *D*: Coacervate protein (phase separated).

2.6 Rheometric Measurements

All rheometric measurements were collected on the Physica MCR 301 Rheometer from Anton Paar. This rheometer, like many others, can perform both rotational and oscillatory tests. Illustrated below in *Figure 2.2* is a brief schematic showing some of the main components and various parts of the MCR 301 rheometer used in this study.

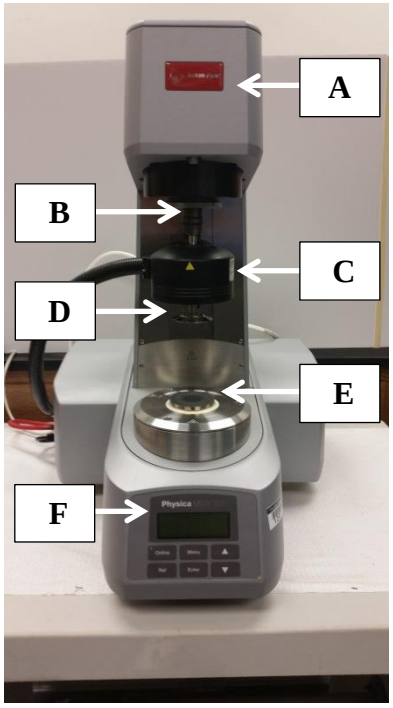

A. Motor assembly: air bearing-supported synchronous motor; permanent magnets to produce constant magnetic field for delay-free responses.

B. Motor shaft: quick-fitting coupling; holds measuring tools in place.

C. Peltier heating hood/ evaporation blocker system.

D. Measuring system tool: various geometries; cone, plate, or bob.

E. Measuring base: sample loading; plate or cup.

F. Display: displays current interval parameter, temperature of base, and gap distance.

Figure 2.2: Schematic demonstrating key components of the MCR 301 Rheometer.

2.6.1 Rheometer Operation Procedures

It was necessary for the electrical components of the rheometer to warm up prior to operation. The rheometer was powered on and allowed a minimum of 30 minutes prior to any tests being performed. Next, the instrument was initialized and the measuring system tool (i.e. cone, plate, or bob) was inserted. It is recommended that a "Motor Adjustment" (which calibrates the motor) is run once every 90 days however; the motor adjustment was performed weekly just as a preemptive measure. Also, a "Measuring System" calibration which determines and calibrates the inertia of the measuring system tool was performed on a daily bases. Prior to any loading of sample it was necessary to set the "Zero Gap" which sets the zero measuring position (applicable to cone and plate and parallel plates geometries).

2.6.2 Loading Sample onto Rheometer

All rheometer tests were completed using a cone (1° angle, 50 mm diameter) and plate geometry. Loading of sample (i.e. ELPs) onto the rheometer was very important (*Figure 2.3*). This was even more important when loading the cone and plate and also the parallel plates measuring tools as inaccurate loading amplifies errors in data measurements. Loading samples onto tools was completed as follows:

> Load sample onto bottom plate. When a sufficient volume of sample is loaded the top cone is lowered to the measuring position. Excess sample is wiped away to insure that loaded sample is in line with the edge of the cone.

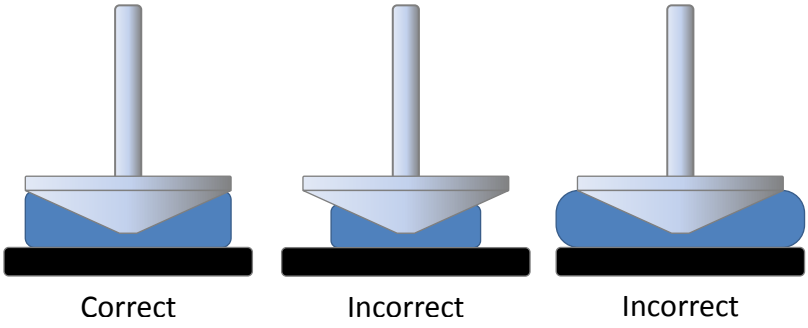

Figure 2.3: Loading procedure for loading sample onto cone and plate (blue represents sample).

2.7 Oscillatory Strain Measurements

When conducting oscillatory strain measurements on a sample it is important to perform the tests in the appropriate order to accurately evaluate the relationships between molecular structure and viscoelastic behavior. The first step is to determine the linear viscoelastic region (LVE) of the material being tested (*Figure 2.4*). To determine this

region, a percent strain sweep, also termed amplitude sweep, must be performed. This test consists of increasing the percent strain from very low to much higher percent strains. This is completed at a constant angular frequency. The determination of the LVE region is important because it allows for the determination of the range of percent strains that are acceptable for use in later tests. If a percent strain is utilized that exceeds the percent strain in the LVE region the mechanical structure of the sample will be compromised and thus the data collected may be inaccurate.

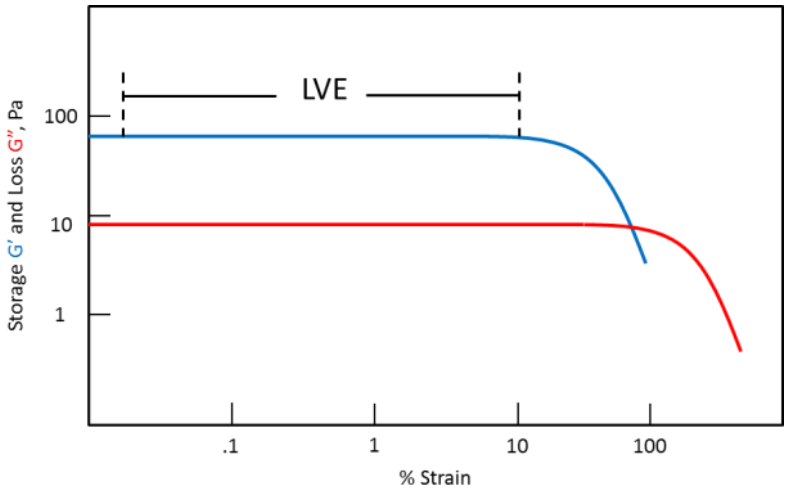

Figure 2.4: Typical plot of LVE region. The point of severe deformation from the linear region can be considered the maximum percent strain of the LVE.

After determining the LVE, a percent strain somewhere within this region will be used in the next test conducted. For example, when examining *Figure 2.4* above, a percent strain anywhere between approximately 0.01 and 10 would be used. The next test that will be performed is a frequency sweep. This test is conducted using a constant strain within the LVE. This type of test consists of varying frequency, f, or more commonly angular frequency, ω. The storage and loss moduli are measured with respect to angular

frequency. Using the data collected the viscous and elastic properties can be examined and characterized.

Other tests conducted included the complex modulus, G^*, the dynamic viscosity, η', the out-of-phase viscosity, η'', the complex viscosity, η^*, and the damping factor, $\tan\delta$. All of these preformed tests are representations of the viscoelastic components of a material. Along with the viscoelasticity, important tests were performed to further understand the rheology of the samples. Such test included shear dependency and time dependency which will be explained further in the next chapter. This data used in collaboration with one another allows for proper and complete characterization of the viscous and elastic properties of a material.

2.8 Transition Temperature Measurements

Transition temperatures were measured using a Shimadzu 1800 UV-Visible spectrophotometer. This instrument uses a temperature controlled peltier thermal chamber holding assembly with a cooling water circulating bath to remove excess heat from the system. The sample was loaded into a polymethyl methacrylate (PMMA) cuvette which contained a glass NMR (nuclear magnetic resonance) tube inside surrounded with water (*Figure 2.5*). This assembly was necessary due to the large volume required (approximately 2 ml) when using a regular PMMA cuvette. It would be difficult to provide these large sample sizes when working with highly concentrated ELPs. When using the apparatus shown below the required minimum sample size is reduced to only 200 μL. The NMR tube is removable which allows for centrifugation.

This is necessary when getting the highly viscous protein samples to the bottom of the NMR tube.

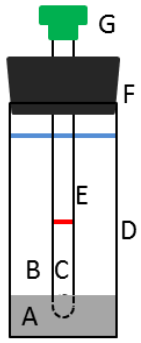

Figure 2.5: Cuvette with NMR glass tube used in transition temperature measurements. *A*: Resin to hold bottom of NMR tube in place. *B*: Water filling void between cuvette walls and NMR tube walls. *C*: Protein sample. *D*: PMMA Cuvette. *E*: Glass NMR tube. *F*: Rubber stopper to hold top of NMR tube in place. *G*: NMR tube cap.

The cuvette assembly was placed into the holding assembly for measurements. A constant temperature ramp of 0.2 °C/minute was used when heating samples in the instrument. This heating rate was used to allow time for the temperature to equilibrate within the system. At a slow rate of heating the effects of temperature lag were minimized. When performing these temperature sweeps the range of temperatures used were 20 °C to 60 °C and in reverse order at a wavelength of 550 nm. A wavelength of 550 nm was chosen because at higher wavelengths the highly concentrated protein does not absorb as much light. To determine this wavelength a spectrum was determined (*Figure 2.6*).

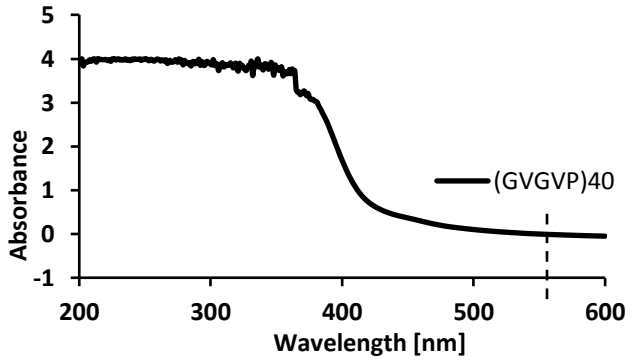

Figure 2.6: Absorbance with respect to wavelength for highly concentrated ELP.

From the spectrophotometer, plots were produced that included the absorbance of light with respect to varying temperature. The purpose of conducting these tests was to determine at what temperature the ELPs exhibit their transition temperature (T_t). When the temperature was increased to a high enough temperature the lower critical solution temperature (LCST) behavior was reached. What was observed at this point was an increase in absorbance. Previous studies [49] used to determine a single temperature as the T_t involves analyzing the midpoint between the onset of turbidity and the absorbance at to peak of the curve. This is shown in the simple equation illustrated below (*Equation 2.2*).

$$\frac{Absorbance_{onset}+Absorbance_{peak}}{2} = Absorbance_{T_t} \qquad Eqn.\ 2.2$$

From the $Absorbance_{T_t}$ calculated the corresponding temperature at that absorbance value gives the T_t.

CHAPTER III

RESULTS AND DISCUSSION

3.1 Rheometric Analysis of Elastin-like Polypeptides

This section examines the viscoelastic behaviors of measurements gathered during the duration of this study. In particular, the elastin-like polypeptide constructs $(GVGVP)_{40}$ and $(GVGVP)_{40}$-foldon were examined using a series of rheometric tests to show the time, shear, temperature, and concentration dependence.

The first experiments performed tested the time dependency of the polymeric systems. When studying the time dependent flow characteristics of a material it is best to use a viscometer or rheometer which impose constant shear rates over the entirety of the sample [42]. In order to achieve this uniform distribution of shear rate a cone and plate geometry is used. For small gap angles the shear rate is nearly perfectly uniform over the

entire sample distribution for the cone and plate geometry (1° angle, 50 mm diameter). When a constant shear is applied to a sample and the resulting viscosity tends to decrease with time, this phenomenon is known as a thixotropic material. Inversely, when the resulting viscosity increases the sample is said to be rheopectic. Samples of $(GVGVP)_{40}$ and $(GVGVP)_{40}$-foldon were subjected to a constant shear over a 20 minute duration to observe if any time dependency exist (*Figure 3.1*).

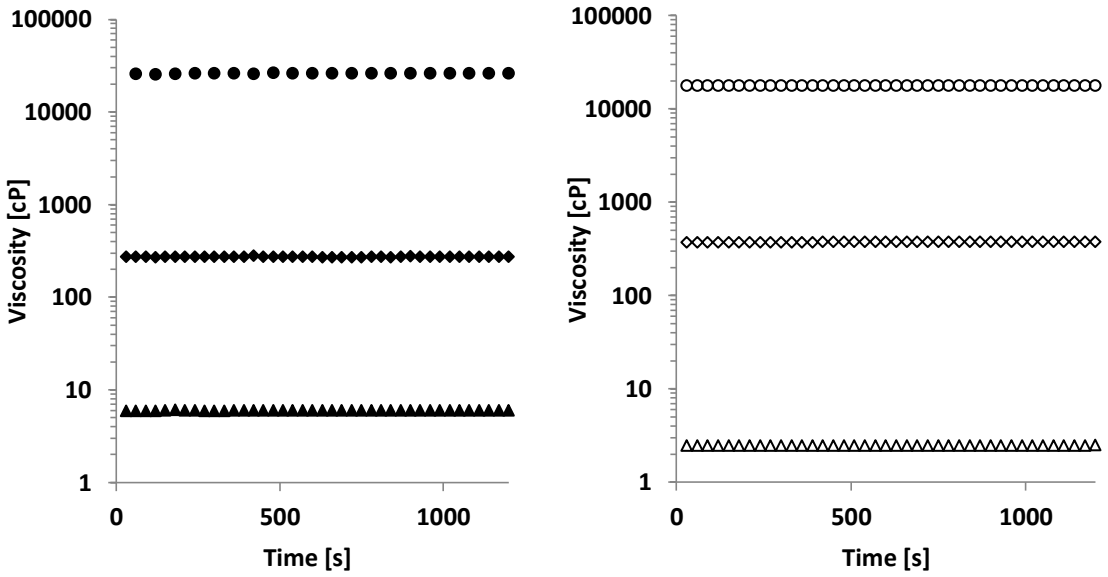

Figure 3.1: Viscosity with respect to time for $(GVGVP)_{40}$ (left graph) at 427 mg/ml (●), 222 mg/ml (♦), and 112 mg/ml (▲) and for $(GVGVP)_{40}$-foldon (right graph) at 383 mg/ml (○), 242 mg/ml (◇), and 99 mg/ml (△) at 20 °C and 100 s^{-1}.

Figure 3.1 shows the time dependency behavior of both the linear and trimerized constructs. All the samples are strained a total of 20 minutes at a constant shear rate. The viscosity remains nearly constant over the full length of time strained therefore, the protein shows little to no time dependency over all concentrations.

Next, the shear dependencies of the systems were examined. From this data it can be determined whether or not a material exhibits Newtonian or non-Newtonian behaviors. Commonly, materials will show some type of change in viscosity with respect to varying shear. When a system shows Newtonian behavior, such as water, it will be independent of shear changes. In other words, as the applied shear rate is varied the resulting viscosity will respond in a linear manner. Another way to determine that a material is Newtonian is if the resulting shear stress with respect to changes in shear strain (or vice versa) shows a linear relationship.

Inversely, if a material exhibits shear dependency (i.e. viscosity changes with respect to shear and shear stress deviates from a linear relation with respect to shear strain) it is said to be non-Newtonian. One common type of a non-Newtonian material is a shear thinning material. As the shear strain is increased the resulting viscosity decreases. This can also be seen as a decreasing deviation from linearity of shear stress versus shear strain (shear rate). A less common type of a non-Newtonian material is referred to as shear thickening. As shear rate increases viscosity increases as well. Also, shear stress will deviate in an increasing manner from linearity with increases in shear strain (*Figure 3.2, 3.4*).

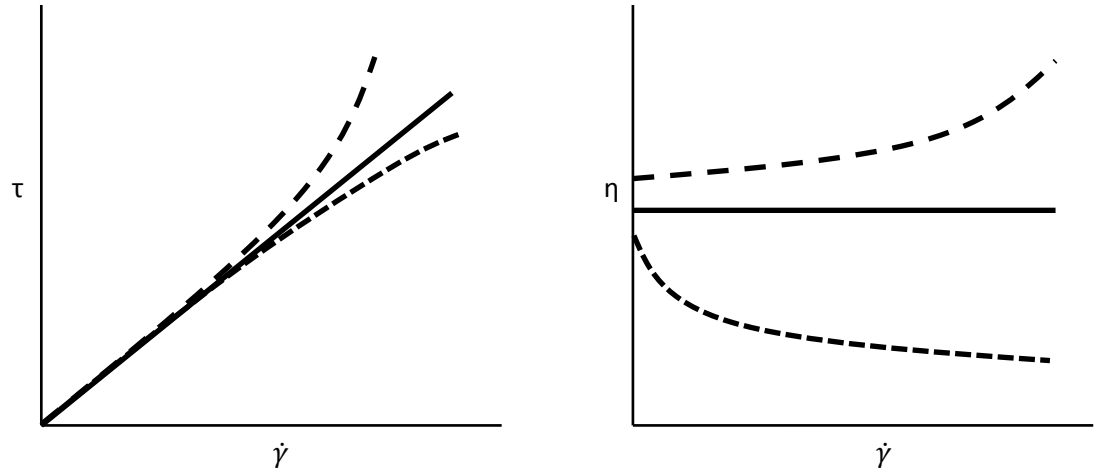

Figure 3.2: Shear stress versus the shear rate and viscosity versus shear rate for Newtonian (solid lines) and non-Newtonian (dashed lines). For the left graph, the upper dashed line represents a shear thickening material while the bottom represents a shear thinning material. Similarly, for the right graph, the upper dashed line represents shear thickening and the bottom represents shear thinning.

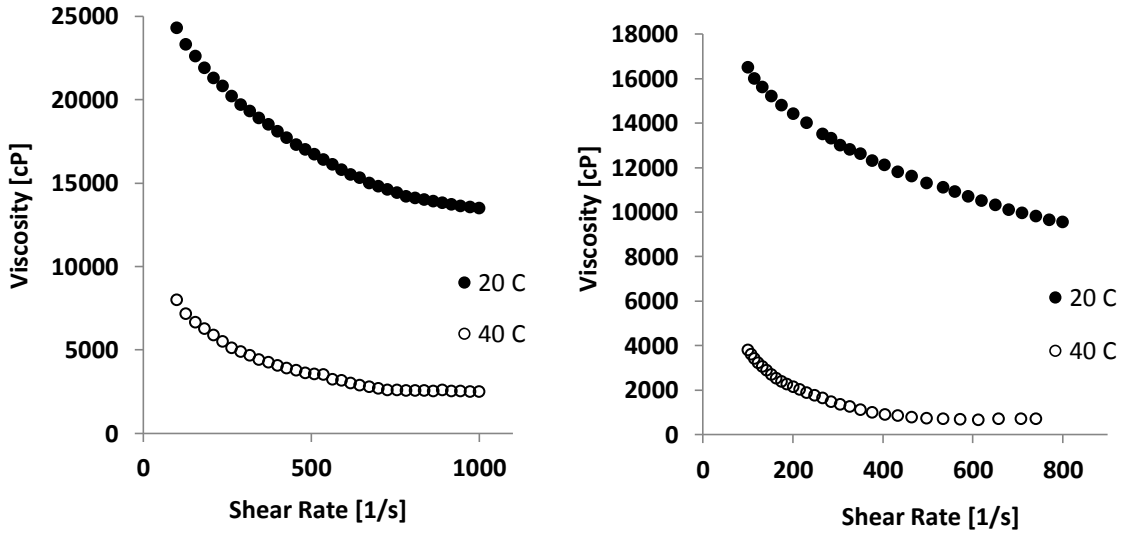

A. **B.**

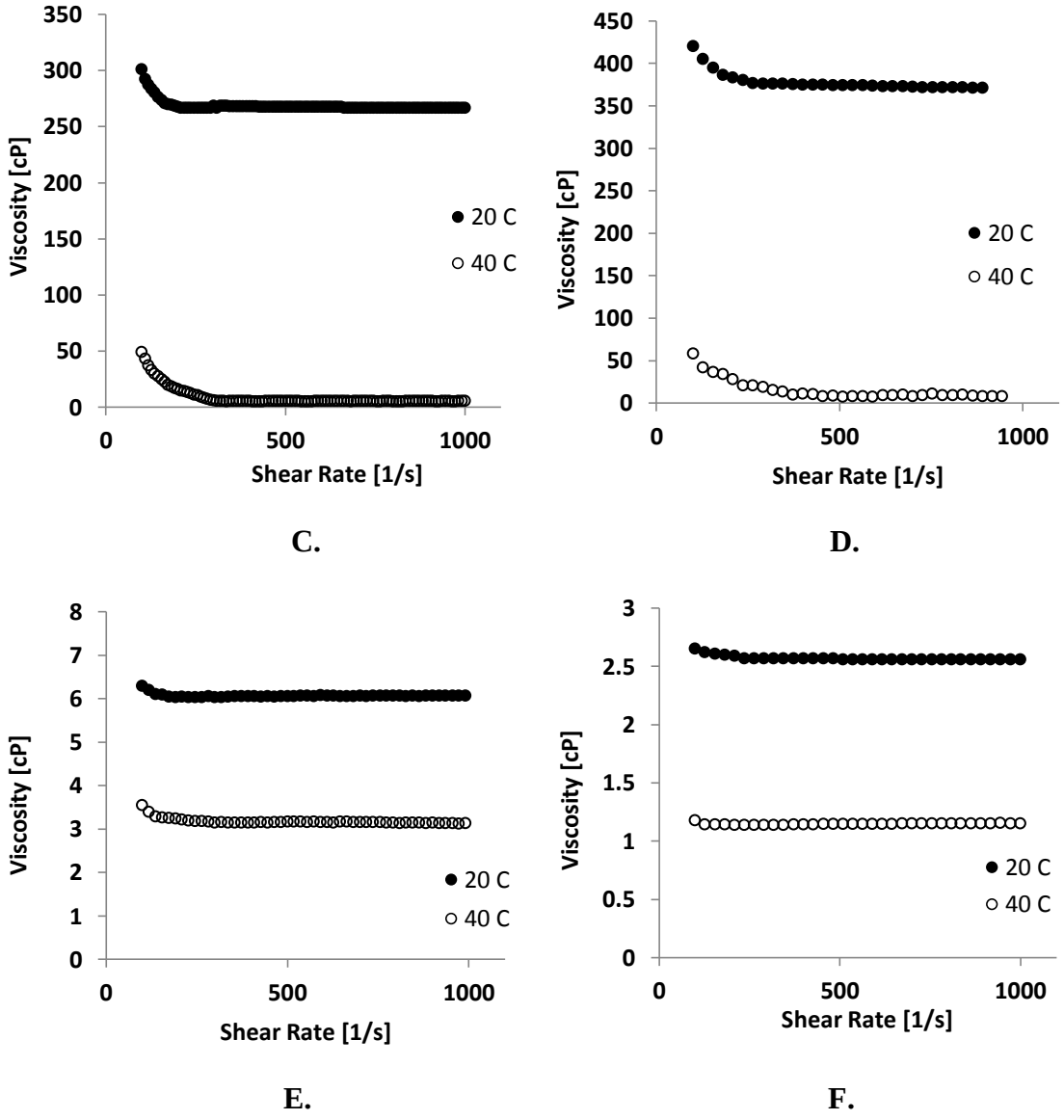

Figure 3.3: Viscosity with respect to shear rate, $\dot{\gamma}$, for $(GVGVP)_{40}$ at 427 mg/ml (*A*), 222 mg/ml (*C*), and 112 mg/ml (*E*) and for $(GVGVP)_{40}$-foldon at 383 mg/ml (*B*), 242 mg/ml (*D*), and 99 mg/ml (*F*) at 20 °C and 40 °C.

Samples of $(GVGVP)_{40}$ and $(GVGVP)_{40}$-foldon at various concentrations and temperatures were examined as a function of shear rate. Shown in *Figure 3.3* is the shear dependency of these two constructs. As can be seen in the graphs, there is a difference in viscosity with respect to shear rate. At the higher concentrations there are large changes in viscosity as shear rate increases. As the systems become more dilute, the magnitudes of change in viscosity decrease. By the last dilution, at 112 mg/ml for the linear protein and 99 mg/ml for the trimer, the magnitude of change is quite small. The system is becoming more and more like water as the concentration of protein is decreased. As mentioned previously, water is Newtonian so viscosity will not change with respect to changes in shear. This explains the near constant (but still slightly decreasing) viscosity of the low protein concentration systems. The viscosity is seen to decrease continuously with increasing shear, thus showing a shear thinning behavior at all dilutions. As the shear rate is increased the chains begin to orient in the direction of the applied shear. This orientation is what decreases the viscosity (i.e. shear thinning behavior) [42].

Cirulis *et al* studied the rheological properties of highly concentrated elastin-like polypeptides to understand post-coacervation changes in structure and assembly [53]. This ELP consisted of three hydrophobic domains of native human tropoelastin flanking two cross-linking domains. The authors study shows a strong shear thinning behavior for the ELP studied. Shear thinning was seen at both high and low temperatures. It was suggested that the behavior observed is due to the alignment by shear forces. This behavior is consisted with what is observed for $(GVGVP)_{40}$ and $(GVGVP)_{40}$-foldon as investigated in this study.

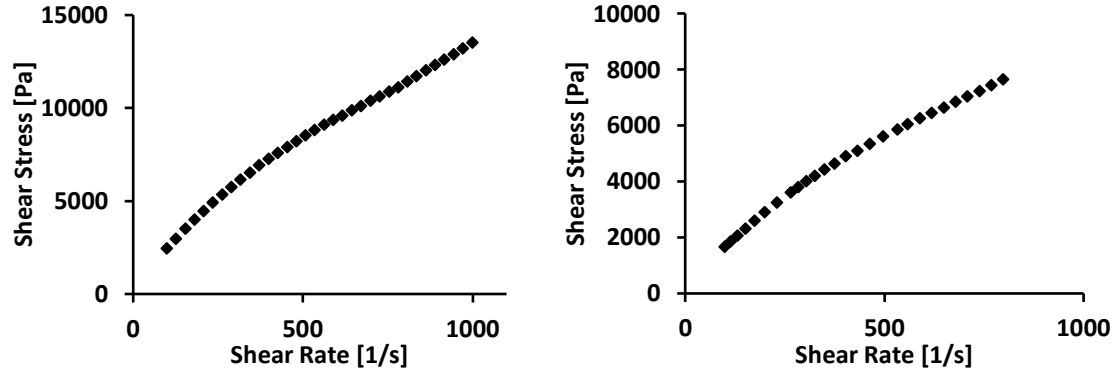

Figure 3.4: Shear stress versus shear rate. Shown is $(GVGVP)_{40}$ at 427 mg/ml (left) and $(GVGVP)_{40}$-foldon at 383 mg/ml (right).

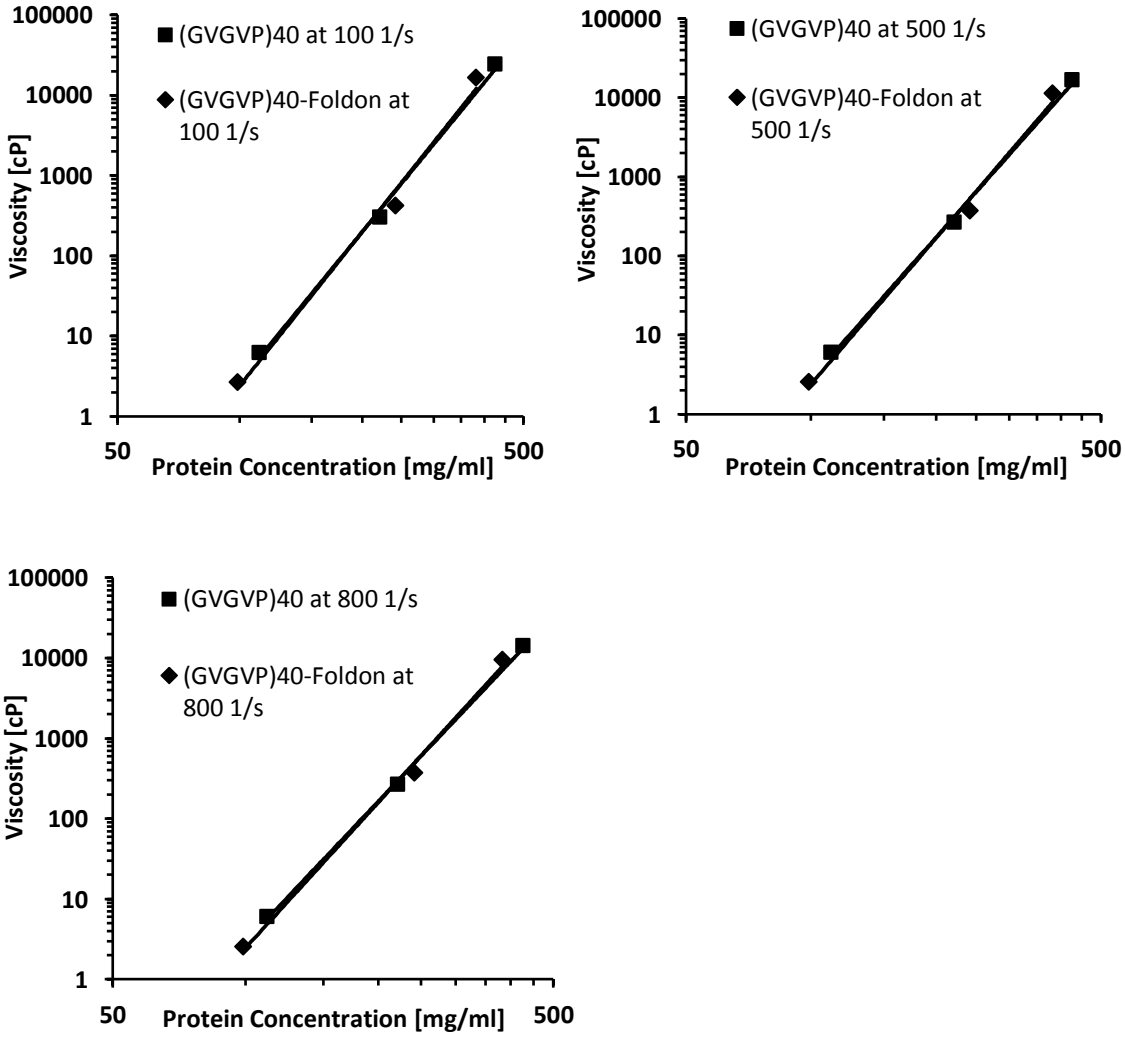

Figure 3.5: Viscosity versus protein concentration.

The viscosity of $(GVGVP)_{40}$ and $(GVGVP)_{40}$-foldon were examined with respect to protein concentration (*Figure 3.5*) at specific shear rates. Applying a log-log scale, the data can be modeled using a power law model. A relationship can be provided from the data such that the viscosity will be equal to a constant multiplied by the concentration to a power (*Equation 3.1*)

$$\eta = kC^m \qquad \textit{Eqn. 3.1}$$

Here, η is viscosity, k is a constant, C is protein concentration, and m is the slope of the line (scaling factor). For the data given in *Figure 3.5*, the equations for the fit of the power law are shown below for $(GVGVP)_{40}$ and $(GVGVP)_{40}$-foldon.

Shear Rate [s^{-1}]	**$(GVGVP)_{40}$**	**$(GVGVP)_{40}$-foldon**
100	$\eta = 1.21\text{x}10^{-12}(C)^{6.18}$	$\eta = 4.84\text{x}10^{-12}(C)^{6.35}$
500	$\eta = 4.18\text{x}10^{-12}(C)^{5.92}$	$\eta = 1.40\text{x}10^{-12}(C)^{6.19}$
800	$\eta = 7.72\text{x}10^{-12}(C)^{5.79}$	$\eta = 2.36\text{x}10^{-12}(C)^{6.01}$

Table 3.1: Power law fits for samples of linear and trimerized ELPs.

The scaling factors for both the linear and trimerized proteins were examined at three different shear rates. The two proteins show similar scaling factors compared to one another. Comparing shear rates to one another, it is observed that as the shear rate is increased the scaling factor decreases (i.e. effect of concentration has a more significant effect at lower shear rates compared to higher shear rates). It was also observed that at

each shear rate examined the two proteins show similar scaling factors however, the trimerized proteins scaling factor remained slightly higher (i.e. trimerized protein tends to have a slightly larger effect on viscosity with increasing concentration compared to the linear protein).

It has been shown that many polymer systems show a power law relation at high polymer concentrations [52, 55]. Phillies studied the power law model fit for 23 polymer-solvent systems. The scaling factors that were observed for the polymer systems ranged from 3.91 to 8.4 [50]. The scaling factors observed for the two constructs of elastin-like polypeptides are acceptable as they fall within the typical range for polymer-solvent systems.

For the next experiments, the proteins viscoelastic behaviors were examined. As mentioned previously, when a material is viscoelastic it shows both viscous (loss of energy under applied stresses) and elastic (retention of energy under applied stresses) behaviors. This type of behavior is typical of most polymeric systems to different extents. One common technique for testing for this property is to use controlled sinusoidal oscillatory strains (or stresses) and measuring a resulting stress (or strain) shifted by some phase angle as described in Chapter I. Using these stresses and strains the dynamic moduli are defined and used in characterization of viscoelastic systems.

When performing sinusoidal oscillatory tests it is important to first determine the linear viscoelastic region (LVE). Recalling *Figure 2.4*, this is the region in which little to no deviation is observed for G' and G'' with increasing percent strain at a constant

frequency. Demonstrated below in *Figure 3.6* is an example of the LVE for $(GVGVP)_{40}$ at high concentrations of protein.

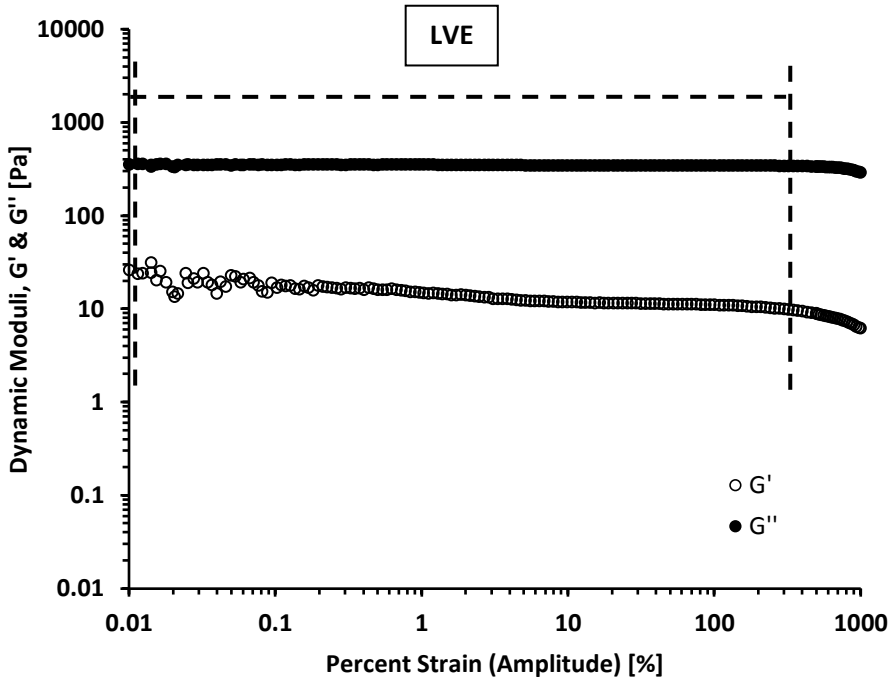

Figure 3.6: Example of amplitude sweep representing dynamic moduli with respect to increasing percent strain for $(GVGVP)_{40}$ at 427 mg/ml. Here, a clear linear viscoelastic region can be observed for percent strains of 0.01 to approximately 300 %.

The next type of test that was performed was angular frequency sweeps. Using a percent strain that lies within the LVE (between 0.01 and 300 % for the example provided in *Figure 3.6*), frequency is varied at a constant percent strain and a number of different properties can be measured. Two of the most common of these properties are the storage and loss moduli (G' and G'' respectively). To test for these dynamic moduli the sample is subjected to a high frequency first and then decreased logarithmically. Using the magnitudes and curvatures of both moduli as a function of frequency the mechanical

characteristics can be described such as degree of viscous behavior compared to elastic behavior.

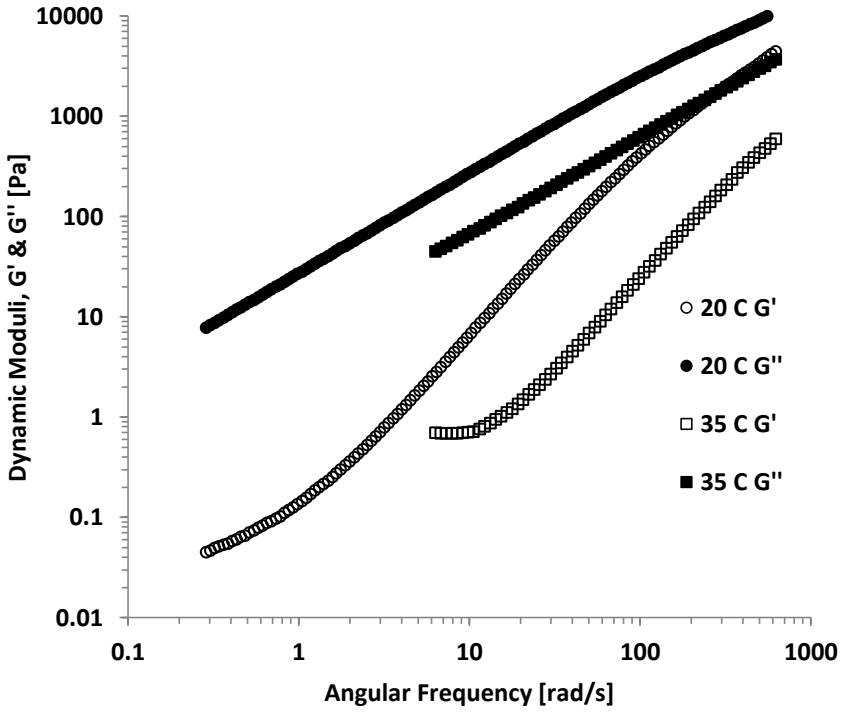

Figure 3.7: Example of the storage (open symbols) and loss (closed symbols) moduli versus frequency for $(GVGVP)_{40}$ at 20 °C and 35 °C.

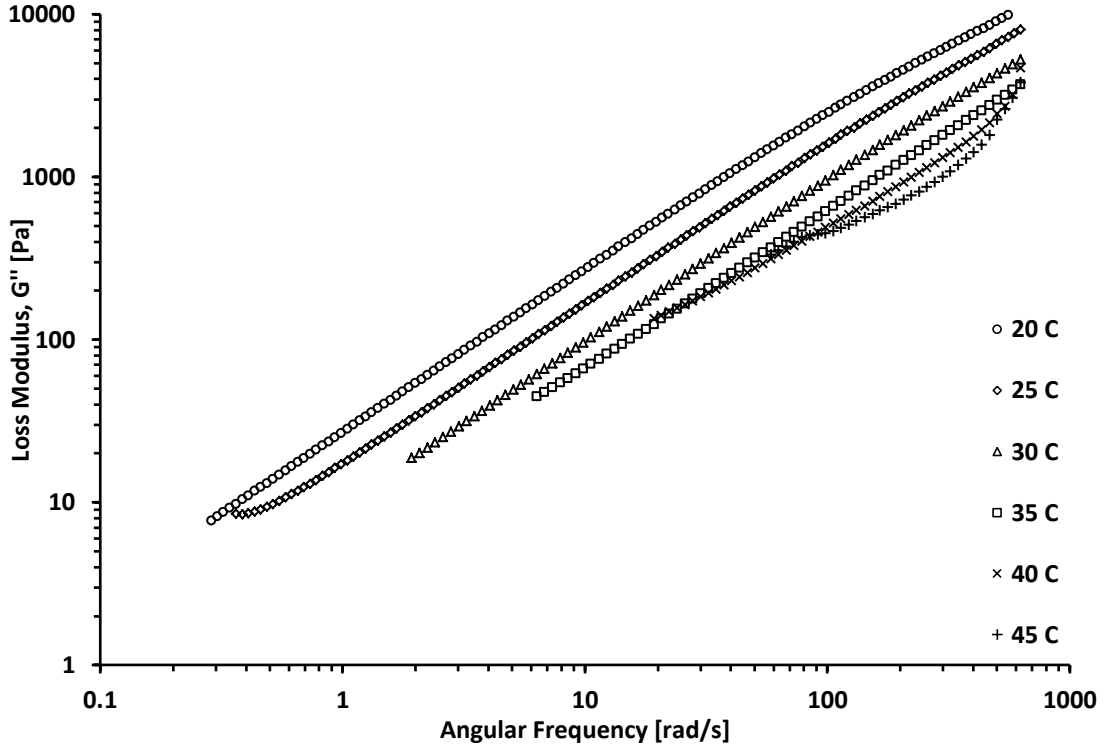

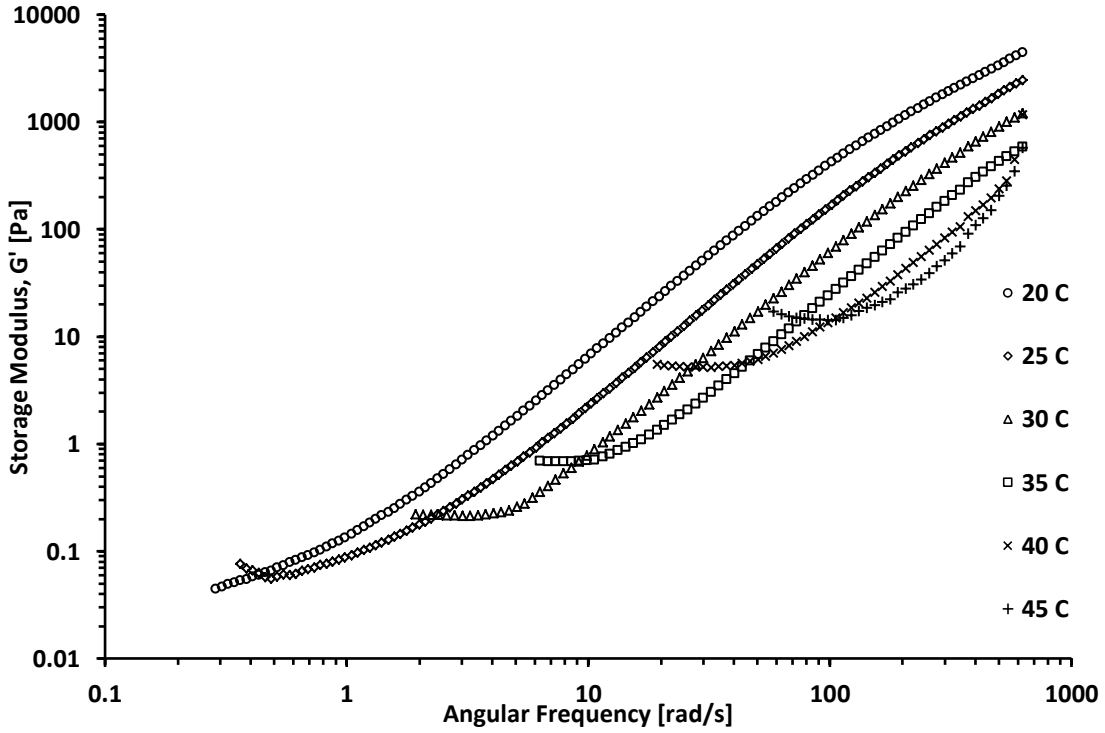

Figure 3.8: Dynamic moduli with respect to angular frequency for 427 mg/ml $(GVGVP)_{40}$. Temperatures range from 20 °C to 45 °C.

In *Figure 3.8*, the temperature dependency on the viscoelastic behaviors was examined at a high protein concentration of $(GVGVP)_{40}$ at 427 mg/ml. The figure demonstrates the behaviors of the loss modulus (top graph) and storage modulus (bottom graph) with respect to frequency at temperatures starting at 20 °C and increasing by increments of 5 °C to a temperature of 45 °C. For all temperatures, over all the frequency ranges tested, the loss modulus is always greater than its respected storage modulus (i.e. no crossover points exist). Therefore, it can be said that this system has more viscous behaviors than it does elastic behaviors. Also, there exists no transitioning to a gel state therefore the system remains as a solution at all frequencies.

The loss modulus tends not to deviate significantly from linearity on the log-log scale graphs. However, at temperatures above 35 °C, the loss modulus tends to show some deviation from this behavior as it begins show an upwards curvature with increasing frequency. It should also be noted that as the temperature of the system was increased the loss modulus decreased indicating a decrease in viscosity with temperature. When examining the elastic behavior of the system, storage modulus, there are more changes with respect to frequency compared to that of loss modulus.

There are two evident and distinct trends that can be seen. First, there exist some minima for each temperature (aside from 20 °C due to the test not being carried out to a low enough frequency) in which the storage modulus reaches a minimum value at a specific frequency. For example, for the 25 °C run this minimum exists at approximately around 0.5 rad/s. As the temperature increases these minima occur at larger frequencies and at a greater magnitude of storage modulus. The second clearly visible trend is a transition from a curvature upwards to a curvature downwards. *Figure 3.9* focuses on

frequencies around 10 rad/s to 1000 rad/s (looking at this figure in collaboration with *Figure 3.8* it is easier to see this trend). From 20 °C to 30 °C the storage modulus tends to have an increasing behavior which begins to deviate in a downwards fashion around where the arrow is shown in this figure. At 35 °C this behavior is no longer existent and shows a nearly linear relationship (aside from the previously mentioned minimum at lower frequencies). At temperatures, greater than 35 °C, there is a shift in the opposite direction of the behavior of the storage moduli. It can be seen that instead of an increasing behavior that transitions into a decreasing behavior of the storage moduli such as the lower temperatures, there is a constantly increasing behavior. This may be explained by a phase transition at 35 °C which will be discussed further in section *3.2*.

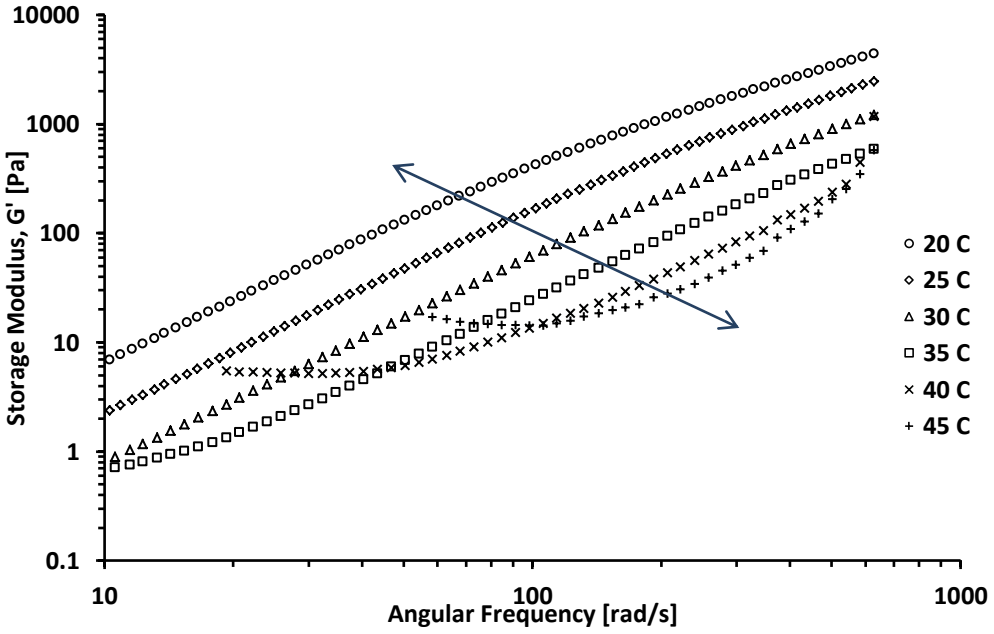

Figure 3.9: Close view on the region demonstrating a shift in behavior of the storage modulus at various temperatures for $(GVGVP)_{40}$ at 427 mg/ml.

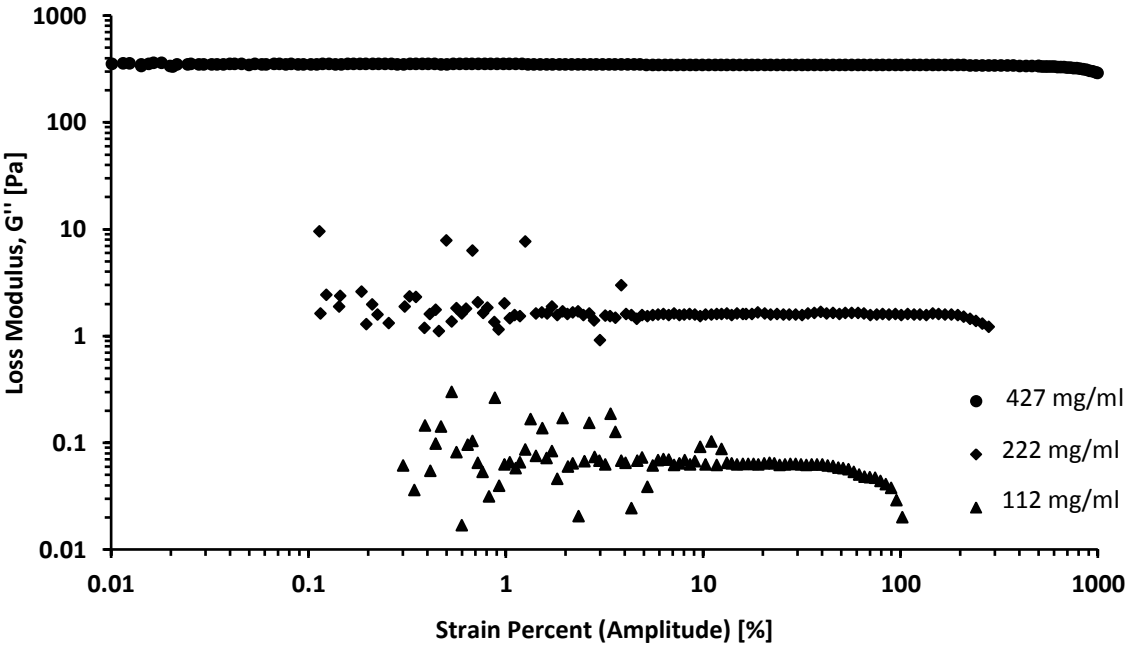
1000
100
10
1
0.1
0.01
Loss Modulus, G'' [Pa]
0.01
0.1
1
10
100
1000
Strain Percent (Amplitude) [%]
427 mg/ml
222 mg/ml
112 mg/ml

A.

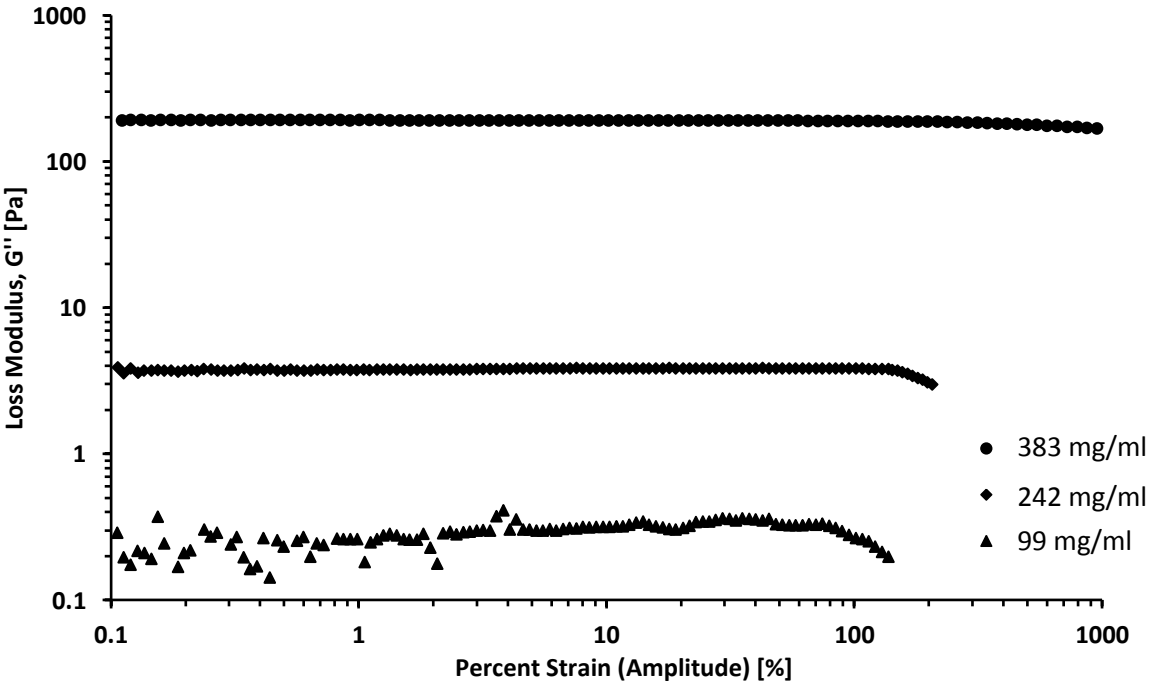
1000
100
10
1
0.1
Loss Modulus, G'' [Pa]
0.1
1
10
100
1000
Percent Strain (Amplitude) [%]
383 mg/ml
242 mg/ml
99 mg/ml

B.

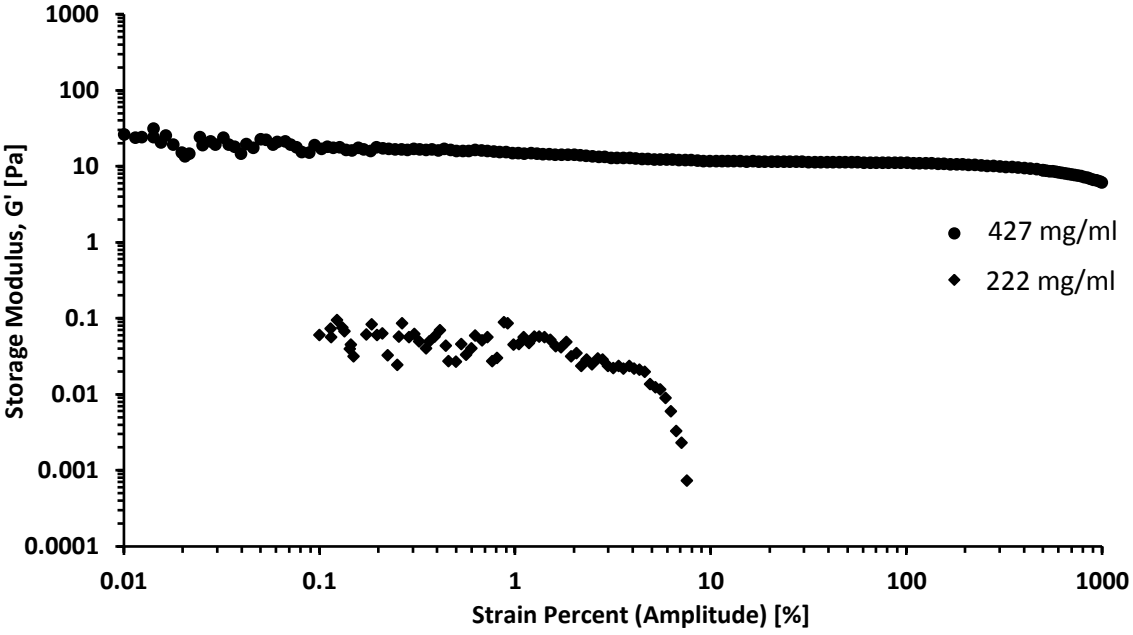

C.

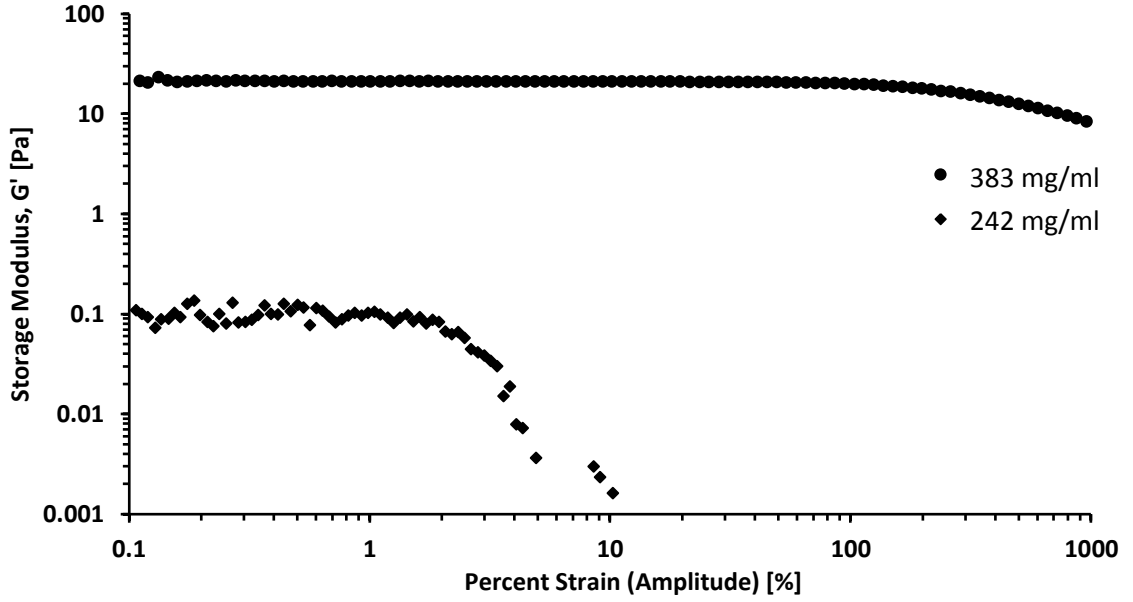

D.

Figure 3.10: LVE regions for various concentrations of $(GVGVP)_{40}$ (graphs *A* and *C*) and $(GVGVP)_{40}$-foldon (graphs *B* and *D*). These regions are obtained by increasing the percent strain (or amplitude of cone oscillation) and measuring resulting storage and loss moduli at 20 °C.

The next study conducted was to examine the effects of concentration on the viscoelasticity of both $(GVGVP)_{40}$ and $(GVGVP)_{40}$-foldon. In order to test for changes in viscoelasticities, the first tests performed were amplitude sweeps at three different concentrations from high to low. Provided in *Figure 3.10* is the loss modulus (*A* and *B*) and storage modulus (*C* and *D*) with respect to increasing percent strain. For each decrease in concentration, for both $(GVGVP)_{40}$ and $(GVGVP)_{40}$-foldon, the loss and storage moduli decrease. The linear viscoelastic regions for each concentration were determined and used for in later tests when performing frequency sweeps at regions lying within these LVEs.

Using the percent strains that were determined from *Figure 3.10* the loss and storage moduli were determined with respect to angular frequency. The results of the dynamic moduli with respect to angular frequency (i.e. frequency sweeps) are displayed in *Figure 3.11*. For both the linear and the trimerized proteins the storage and the loss moduli decrease with decreasing concentrations. The general shape and curvature of the systems is what may be expected for these types of polymeric systems [42]. The magnitudes of the moduli are continuously increasing with increase in angular frequency. For these polymeric systems the magnitude of the loss modulus is always larger than that of the storage modulus. This indicates that the system behaves more as a viscous material than an elastic material and remains a solution. In other words, the systems exhibit higher levels of viscous behaviors rather than elastic behaviors. This behavior was also observed by Cirulis *et al* when the dynamic measurements of an ELP system were investigated [53]. The authors determined that the loss modulus dominated the storage modulus over all frequencies.

At the lower frequencies there are around two orders of magnitudes difference between the loss and storage modulus. At higher frequencies the difference is reduced to approximately one order of magnitude due to the "S" type curvature of the storage modulus. This shows that the system is becoming more elastic however, not surpassing the viscous behaviors of the polymers.

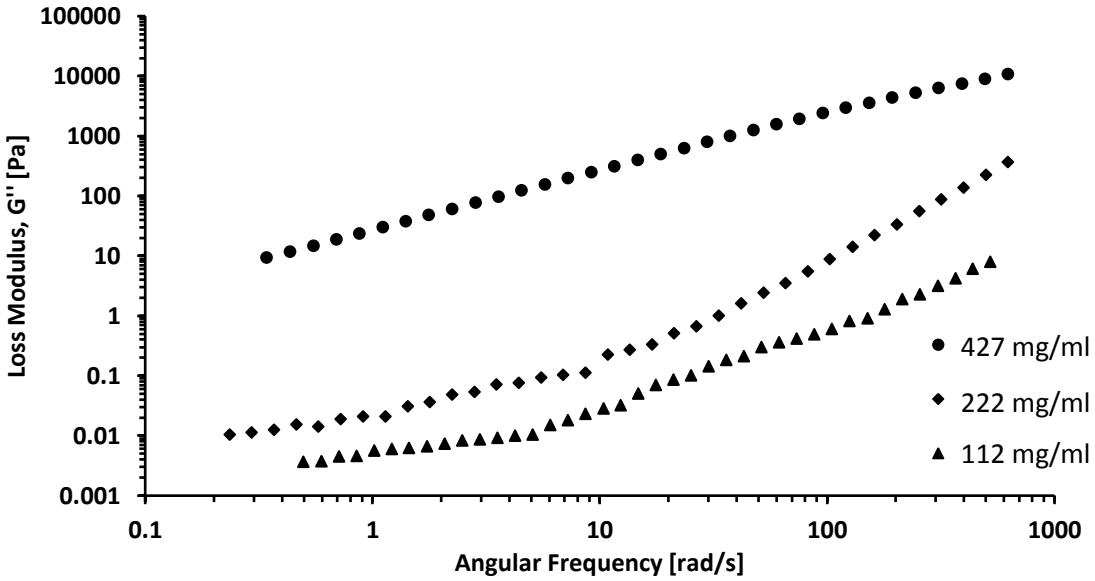

A.

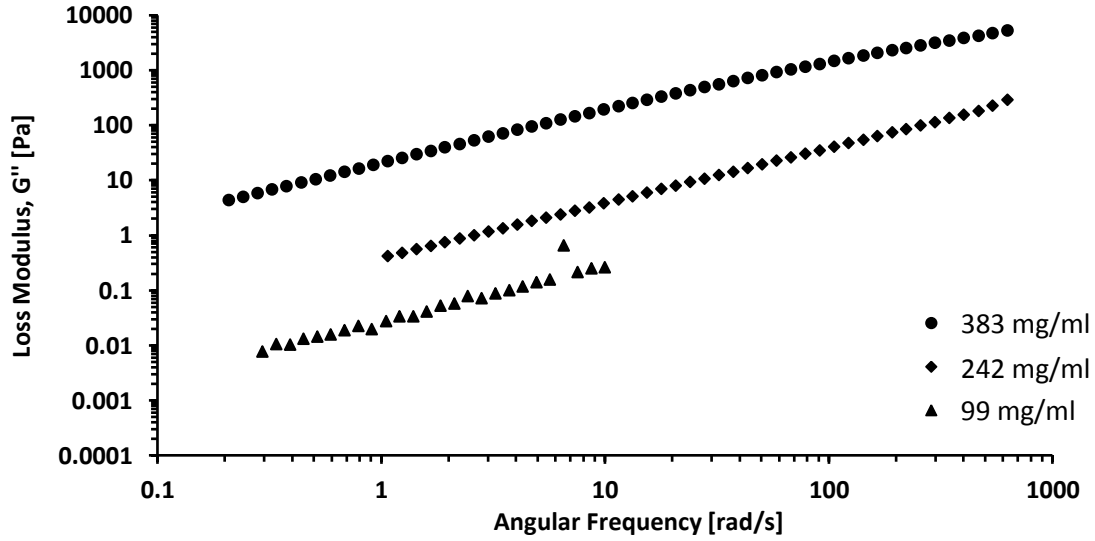

B.

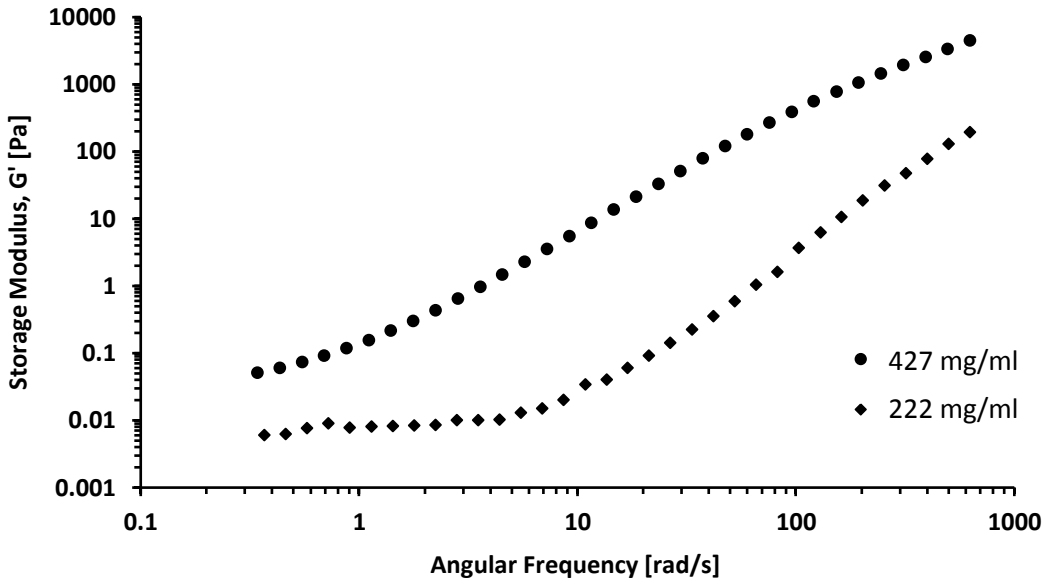

C.

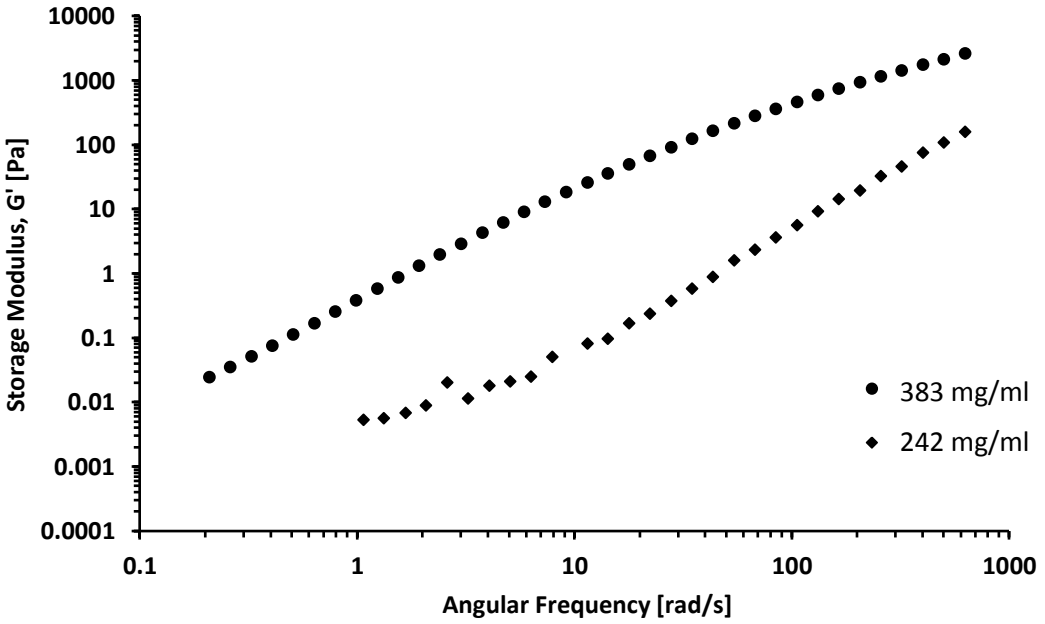

D.

Figure 3.11: Frequency sweeps for various concentrations of $(GVGVP)_{40}$ (*A* and *C*) and $(GVGVP)_{40}$-foldon (*B* and *D*). Using the LVE regions determined from the graphs in *Figure 3.10*, percent strains were determined and used when conducting these frequency sweeps at 20 °C.

3.2 UV-Visible Spectrophotometry Phase Diagram Analysis

As discussed previously, elastin-like polypeptides exhibit phase transitioning behavior. As the temperature of the system is raised from a temperature below the T_t to a higher temperature exceeding the T_t there is a transition from a single phase to a two phase system. These changes are dependent on a variety of properties of the system. The concentration plays a major role in the manipulation of the transition temperature. To better understand the concentration dependence phase diagrams were constructed.

Using the UV-Visible spectrophotometer with the apparatus shown in *Figure 2.5* the temperature was increased at a rate of 0.2 °C/min and the resulting absorbance was recorded.

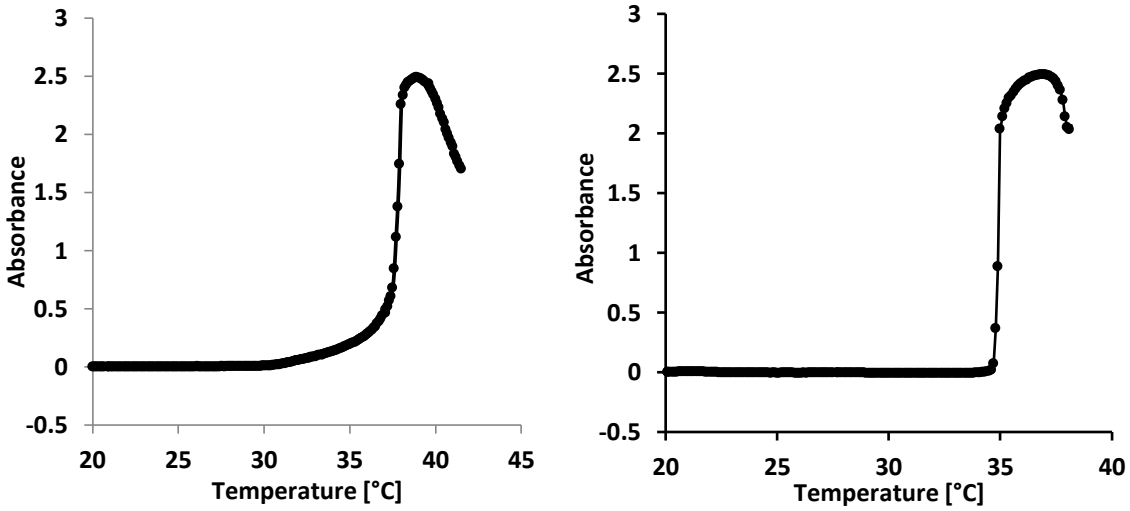

Figure 3.12: Sample absorbance curves for $(GVGVP)_{40}$ at concentrations of 324 mg/ml (left) and 154 mg/ml (right) with at ramp rate of 0.2 °C/min.

Starting at high concentrations around 427 mg/ml, a sample of $(GVGVP)_{40}$ was diluted a total of 22 times. After each dilution the change in absorbance with respect to

temperature was examined (*Figure 13)*. The absorbance tends to remain at the baseline until a deviation is absorbed at the onset of turbidity (*Figure 3.12*). A sudden increase in absorbance is then observed which reaches a maximum peak. For most concentrations the absorbance then tends to drop most likely due to settling of protein after the rapid changes leading to the spontaneous jump in absorbance (which will be discussed further). Using the absorbance curves generated the transition temperature was determined for each concentration of protein. Due to the nature of the curves at different concentrations the transition temperature calculations were examined using several different approaches. One approach for calculating T_t that has been previously used is a "mid-point" method as described by *Equation 2.2*. This method takes the absorbance at the onset of turbidity and the peak of turbidity and averages to the two and the corresponding temperature is the transition temperature. This method works for well for spontaneous increases in absorbance (nearly vertical changes) but not well when there are slow gradual increases as was the case for many of the concentrations studied.

The first technique that was implemented made use of the slope of the curves. As can be observed in *Figure 3.12* there exist a very sharp and sudden increase in absorbance (i.e. approximately 37.5°C (left) and 35 °C (right)) at specific temperatures. It is desired to determine where the tangent line intersects with the baseline absorbance at the steepest slope along the curve. In order to systematically determine this transition temperature, an algorithm was created which calculates the point at which the tangent lines for the entirety of the absorbance curves cross the x-axis (i.e. the absorbance baseline at zero absorbance). For each x-intercept the points were plotted with respect to

temperature. Using the curves generated, the x-intercept at the maximum peak corresponds to the transition temperature (red circle in *Figure 3.14*).

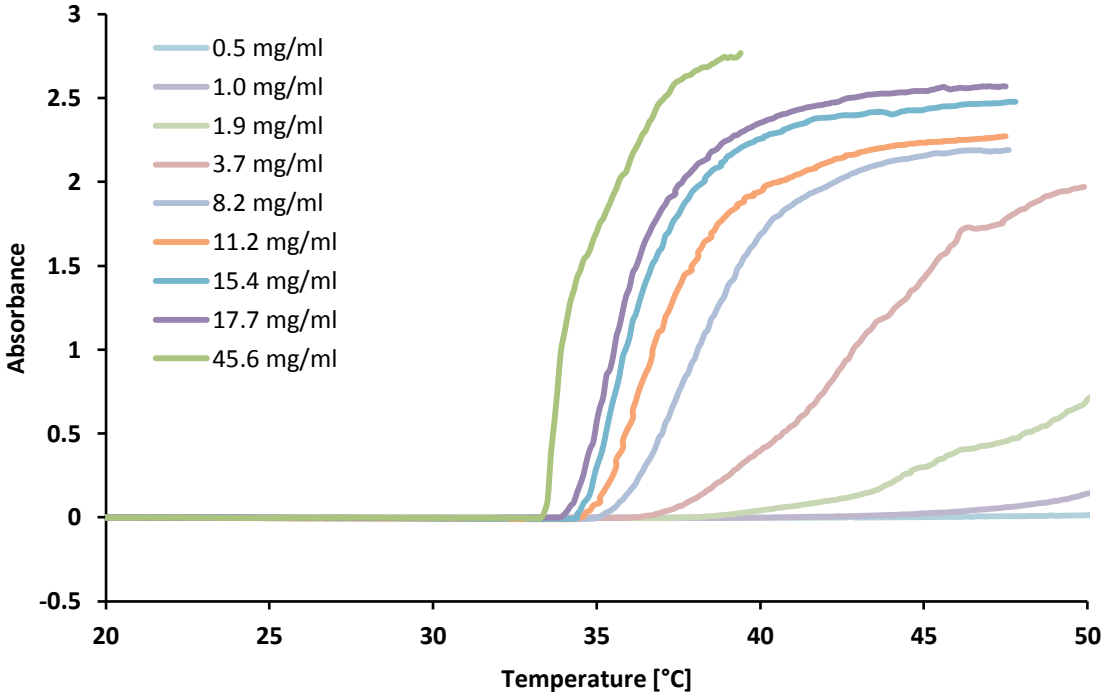

A.

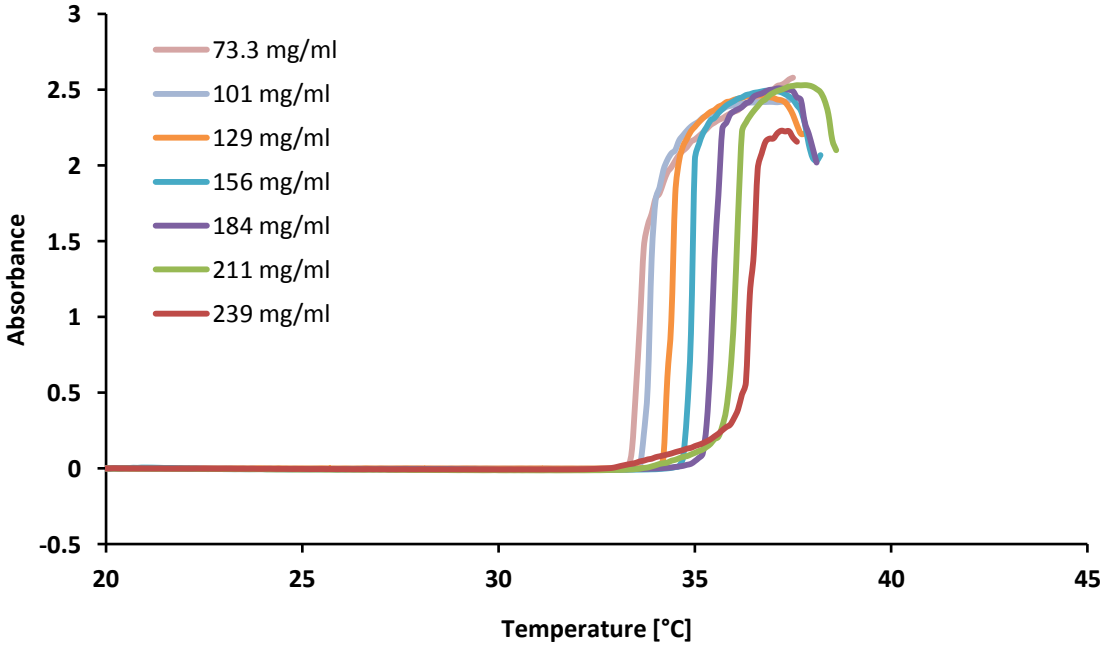

B.

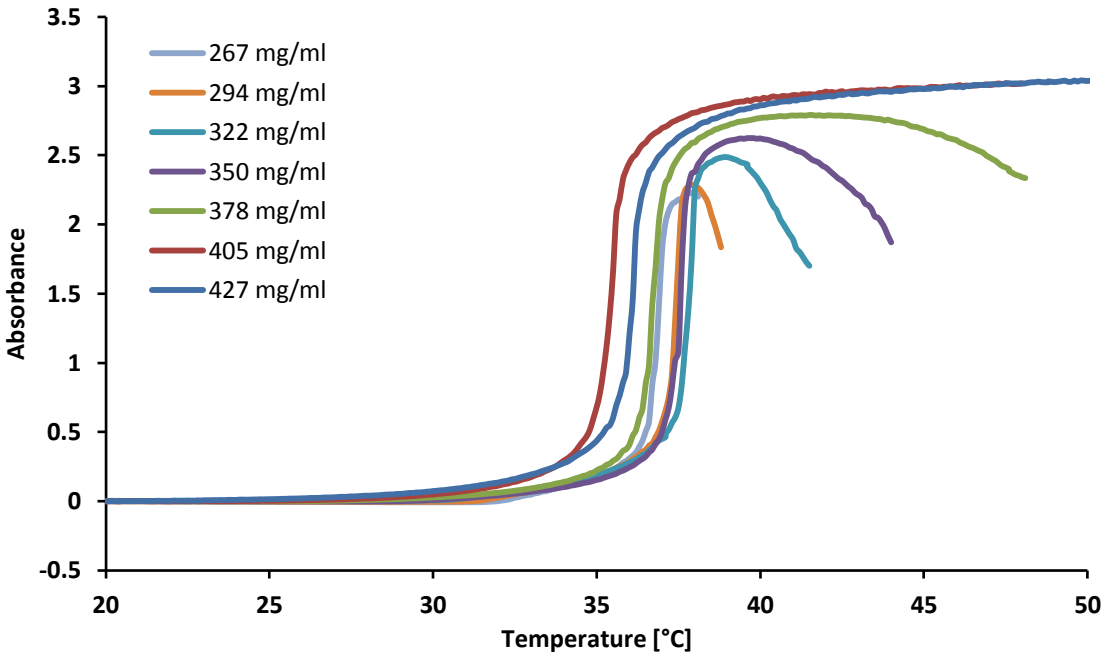

C.

Figure 3.13: Absorbance versus temperature for $(GVGVP)_{40}$. In *A*: concentrations of 0.5 mg/ml to 46 mg/ml, *B*: concentrations of 73 mg/ml to 239 mg/ml, and *C*: concentrations of 267 mg/ml to 427 mg/ml.

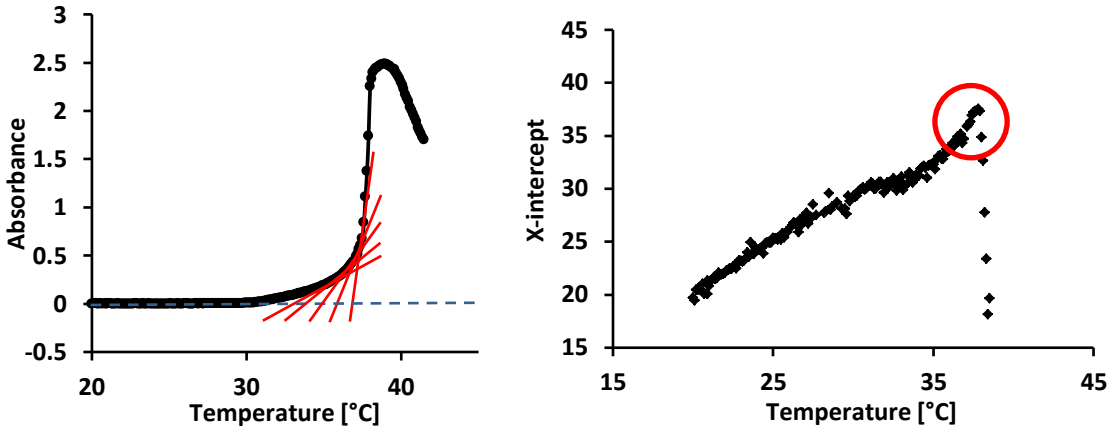

A. **B.**

Figure 3.14: Tangent line method for determining transition temperature. The graph shown on the left (*A*) demonstrates the intersection of the tangent lines (solid red) to the baseline (dashed blue) for $(GVGVP)_{40}$ at 324 mg/ml. These intersections are then plotted with respect to temperature to give the right graph (*B*). The maximum intercept (i.e. 37.6 °C for this sample) is the transition temperature.

The tangent line method described was applied to each absorbance versus temperature curve. Using all of these points together a phase diagram was constructed (*Figure 3.15*). Before examining and explaining the phase diagram shown below alternate methods of determining the phase diagram are discussed.

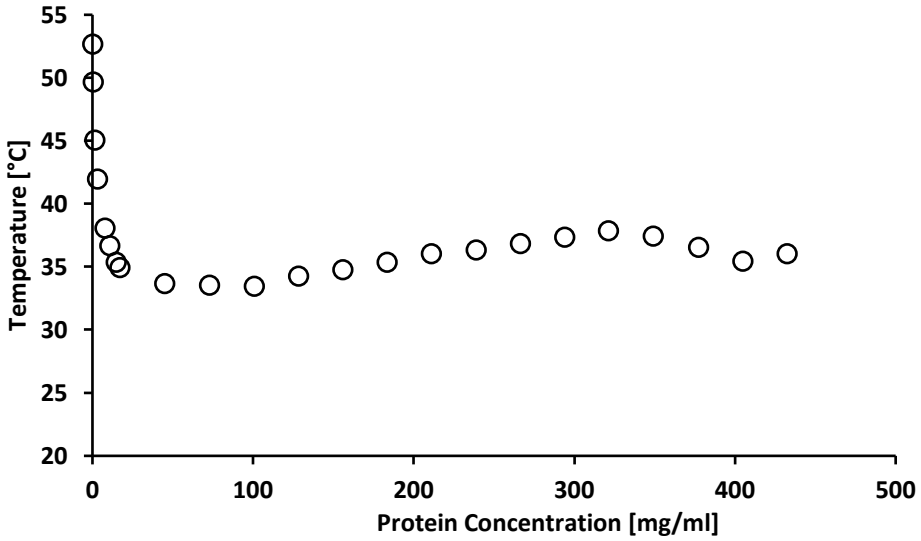

Figure 3.15: Phase diagram created using the tangent line method for $(GVGVP)_{40}$.

To identify the temperature at the onset of turbidity a visual method of analysis was used. For many of the concentrations there exhibits what will be referred to as a "toe" region leading up to the more spontaneous jump in absorbance previously mentioned. This can be clearly seen in *Figure 3.16* below.

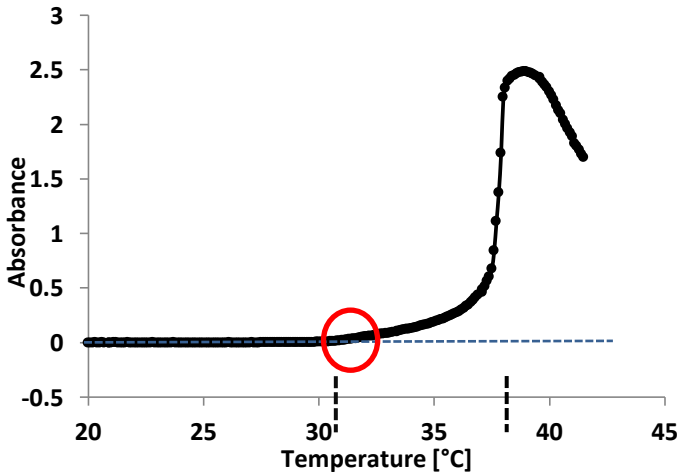

Figure 3.16: Toe region leading up to the spontaneous jump in absorbance for $(GVGVP)_{40}$ at 324 mg/ml. The vertical dashed lines represent the range in which the toe

behavior is observed. The red circle indicates the initial deviation from the baseline (blue horizontal dashed line).

At each concentration of $(GVGVP)_{40}$ the absorbance versus temperature curves were examined using the visual method of analysis described in *Figure 3.17*. The red circle shown in the above figure is the initial deviation of the absorbance curve from the baseline at zero absorbance. Zooming in near these points of deviation a transition temperature was determined for each curve and a phase diagram was constructed (*Figure 3.17*).

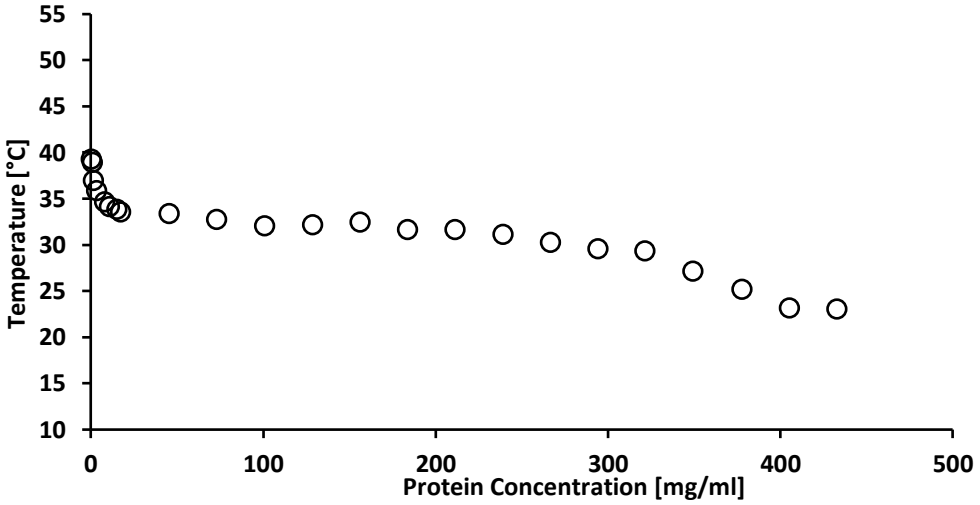

Figure 3.17: Phase diagram created using the visual method of analysis for $(GVGVP)_{40}$.

Another method proposed in order to make the identification of the onset of the toe less subjective was similar to that of the tangent line method described initially. This next method, the modified tangent line method, uses the same slope and tangent line method of calculating where the tangent line intersects the x-axis (baseline). In the previous method the temperature corresponding to the maximum peak (represented by the red circle in *Figure 3.14 B*) is the transition temperature. For this new method, the

same curve is used however the temperature corresponding to the peak is not taken as the transition temperature. Examining *Figure 3.18* below, there exists a region in which a "dip" is observed. This dip is the result of the toe region leading up to the spontaneous change.

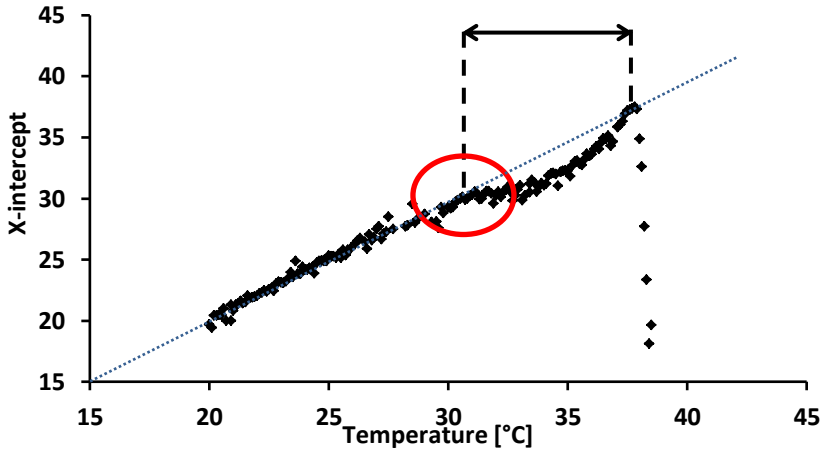

Figure 3.18: Example of the "dip" seen when using the tangent line method represented by the region between the dashed lines. The red circle is the point at which onset of the dip occurs (modified tangent line method).

The initial deviation at the onset of the dip (represented by the red circle in *Figure 3.18*) was examined at all concentrations. The corresponding temperatures were recorded as the transition temperatures at each given concentration. A phase diagram was created using this method (*Figure 3.19*). Using the modified tangent line method the phase diagram has very similar results to that of the visual method of analysis (*Figure 3.20*). What this indicates is that a relatively good representation of the onset of the toe region can be established. The modified tangent line method will be used as the method for determining a transition temperature based on the onset of the toe region.

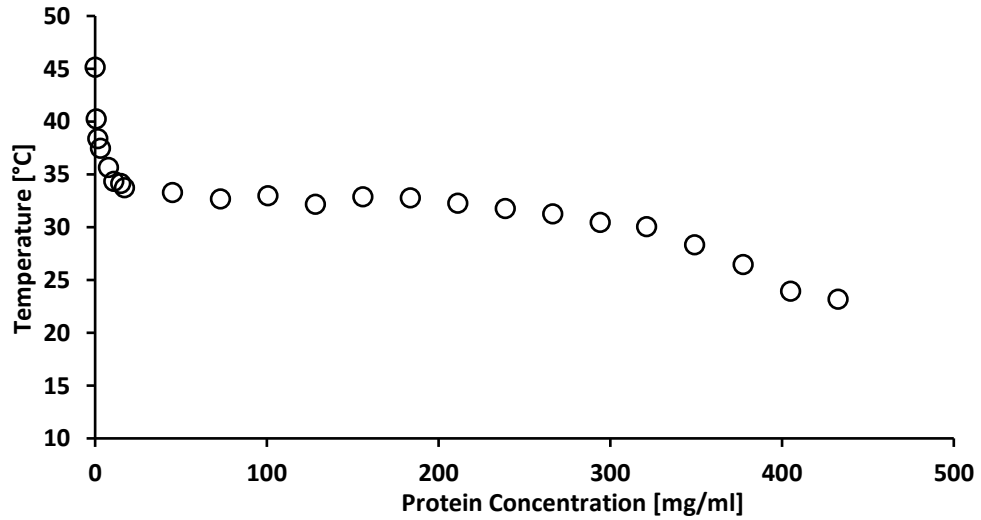

Figure 3.19: Phase diagram created using the modified tangent line method for $(GVGVP)_{40}$.

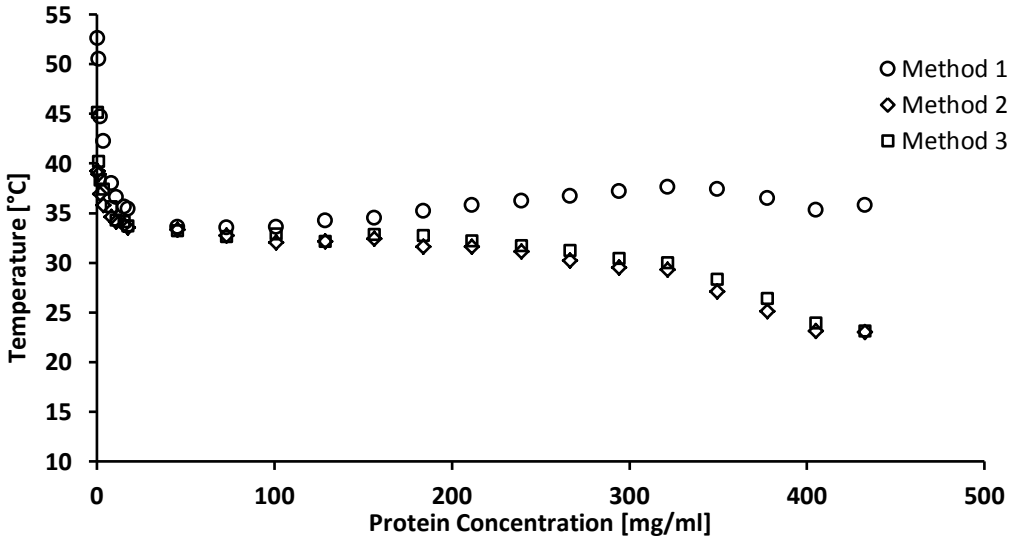

Figure 3.20: Phase diagram for $(GVGVP)_{40}$ using three different methods. Method 1: tangent line method, Method 2: visual method, Method 3: modified tangent line method.

It was desired to check the reversibility of the systems in the toe region. To do this samples of $(GVGVP)_{40}$ were subjected to a temperature increase which was then held and resulting absorbance was examined until equilibrium was reached. The temperature was then decreased stepwise allowing for equilibrium at each temperature until the absorbance reached the baseline. If the system is reversible the absorbance should return to zero (the baseline) at the temperature at which the onset of turbidity is observed.

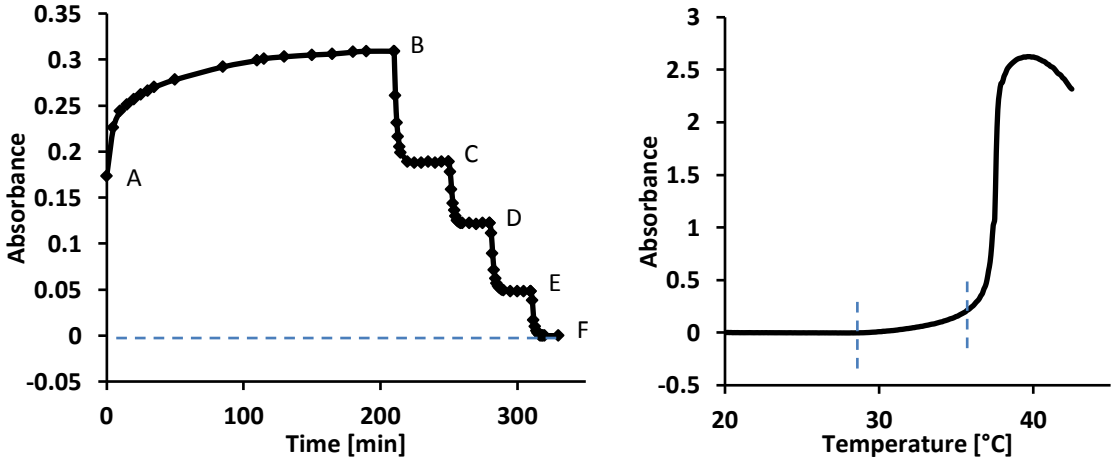

Figure 3.20: Absorbance versus time to check for reversibility. On the left, temperature is increased from 20 to 35.5 °C (*A*) for a sample of $(GVGVP)_{40}$ at 350 mg/ml and the absorbance was allowed to equilibrate. The same process was repeated from 35.5 to 34 (*B*), 32.5 (*C*), 30 (*D*), and 28 °C (*E*) to examine when absorbance returned back to the baseline (*F*). On the right, the dashed line on the left shows the point at the onset of the toe turbidity (28.3 °C) and the right dashed line represents the point at which the temperature was stopped (35.5 °C) to eventually be stepped in the reverse direction.

An example is of $(GVGVP)_{40}$ at 350 mg/ml is discussed (*Figure 3.21*). The temperature was increased to 35.5 °C (*A*) and held. The absorbance was allowed to reach a near equilibrium state and at point (*B*) then the temperature was decreased to 34 °C,

allowed to equilibrate, and repeated for 32.5 °C (*C*), 30 °C (*D*), and 28 °C (*E*). Using the modified tangent line method, the transition temperature was determined as 28.3 °C. Therefore, as the temperature is decreased the absorbance should return to the baseline at 28.3 °C. As seen in the figure above at point (*F*), the absorbance returns to zero at 28 °C confirming the reversibility of the polymer system in the toe region, confirming the accuracy of determining the onset of the toe region.

There is a clear deviation that exists between the more spontaneous behavior described by the tangent line method and the more gradual toe regions described by the modified tangent line methods. There also exists some interesting behavior on all of the phase diagrams described above. Referring to *Figure 3.22* below, at a concentration of 322 mg/ml, the phase diagrams have a shift in curvature. At this point, they tend to show decreasing behavior in the temperature. The samples were placed into the UV-Visible spectrophotometer and heated to temperatures exceeding their transition temperature. For each dilution between protein concentrations of 350 to 433 mg/ml the samples went in as a uniform solution and upon cooling back down to room temperature looked the same as they did prior to heating (right picture of *Figure 3.22 B*).

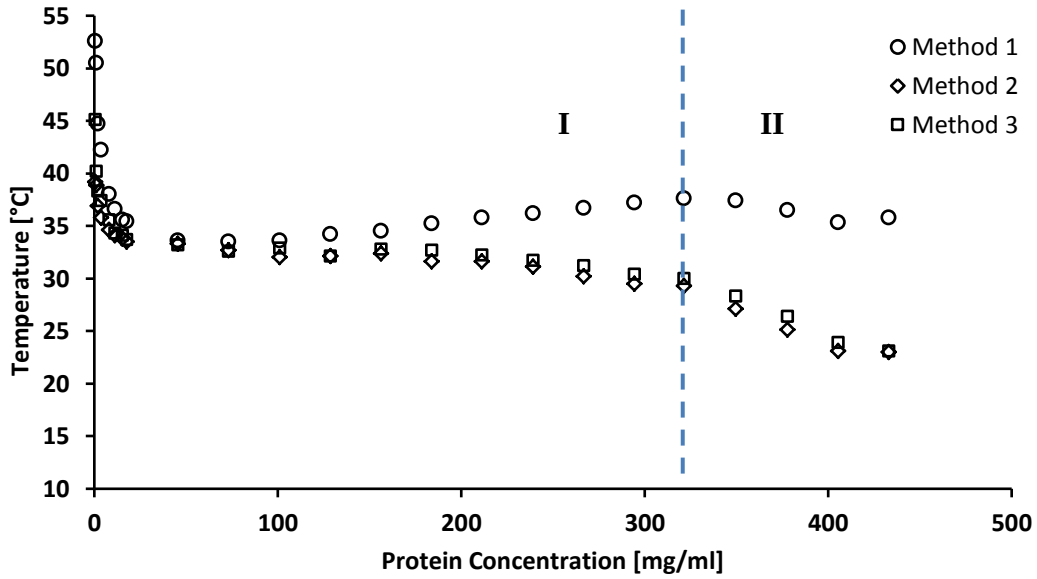

A.

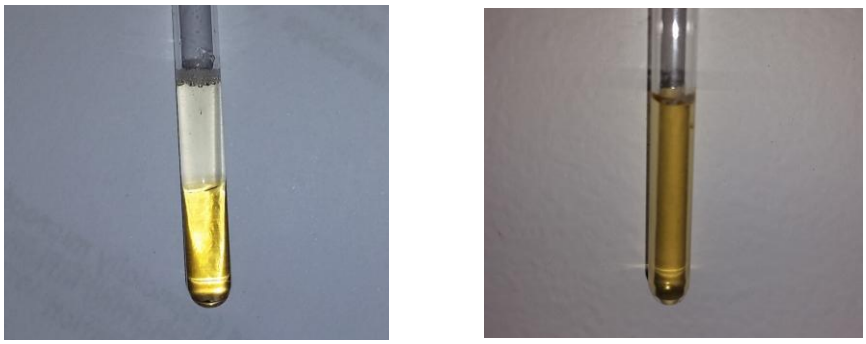

B.

Figure 3.22: Change in behavior observed with increase in protein concentration. Shown in *A* is two regions (separated by the dotted line) observed when constructing the phase diagrams for $(GVGVP)_{40}$. Shown in *B* (left) is a sample of $(GVGVP)_{40}$ at 212 mg/ml from region I at room temperature after being subjected to temperatures above the Tt and (right) a sample of $(GVGVP)_{40}$ at 378 mg/ml from region II subjected to the same conditions.

Upon diluting to concentrations of 324 mg/ml and less (dashed line in *Figure 3.22 A*) the system no longer behaved in the same manner. As mentioned previously, above this concentration the solution started uniform and remained uniform upon heating and then cooling. At a concentration of 324 mg/ml this uniform behavior was no longer observed. Prior to heating the protein solution started as a single uniform phase. The temperature was increased so that it exceeded the Tt of the sample. After the sample was cooled back to room temperature it was no longer a single uniform phase. Referring to the left hand picture in *Figure 3.22 B* a clear separation of phases in observed. On top exists a water rich phase while the bottom consists of a protein rich phase. As each dilution was performed the amount of water rich portion increased as the volume of protein rich sample decreased. This behavior was observed continuously until a concentration was reached in which the solution no longer exhibited the protein rich phase at the bottom of the sample.

The most likely explanation for this change in behavior is due to the changing of continuous phases. At high concentrations there exists a protein rich continuous phase with a water rich dispersed phase. At a concentration of 324 mg/ml these two phases switch to where now the water rich phase becomes the continuous phase and the protein rich phase becomes the dispersed phase (*Figure 3.23*). As the protein rich phase is the continuous phase, the water is unable to move to the surface of the sample. Thus, at concentrations greater than 324 mg/ml there is no water rich phase observed on the surface of the sample after being subjected to high temperatures and cooled back down.

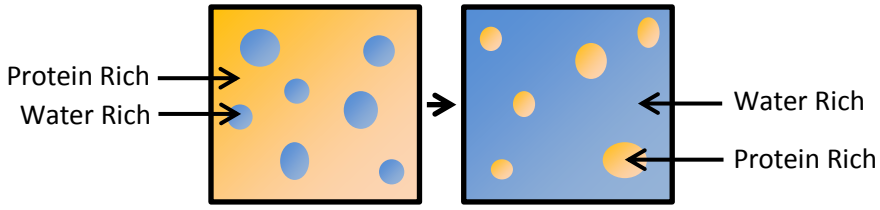

Figure 3.23: Transition from a protein rich continuous phase with a water rich dispersed phase to a water rich continuous phase with a protein rich dispersed phase.

At dilute solutions it is well known that the elastin-like polypeptide $(GVGVP)_{40}$ form aggregates that create a protein rich coacervate. At dilute polymer concentrations the solutions exhibit random polymer coils. Recalling *Figure 1.4*, the random coils in solution begin to become less swollen with increase in temperature. With further increase in temperature the polymer coils exhibit folding and aggregate to form a coacervate.

The dynamics of the highly concentrated solutions as a result of increasing temperature is different than those of the more dilute systems. At high concentrations (Region II) there is significant polymer chain-chain interaction. Due to these interactions, the distribution of the water rich regions of Region I differ from that of Region II. In Region II the system does not tend to interact as significantly with the water.

A model to explain what may be happening in these highly concentrated solutions was proposed. Prior to testing, the solutions are a uniformly distributed system. As the temperature is increased it is believed that there is a formation of water rich droplets distributed throughout the solution. With further increase, the droplets gradually begin increasing in size. Within the system there are chain-chain, water-chain, and water-water interactions. As the temperature of the system is increased, the polymer tends to excrete more water due to hydrophobicity becoming more dominant. As a result, the number of

chain-chain interactions increase therefore, the number of water-water interactions increase as well. The number of water-chain interactions decrease.

When examining the absorbance curves at high concentrations the slow progression of increasing absorbance in the toe regions could be attributed to this gradual increase in droplet size. As the temperature is increased the number of chain-chain interactions increase slowly leading to a slow increase in water-water interactions until the spontaneous increase in absorbance. The polymer chains dictate the dynamics of the system. It is more difficult to move polymer chains then it is for the water to move. As the water droplets grow larger in size the polymer chains need to move to allow for the growth. It is believed that at the point of spontaneous increase in absorbance the polymer chains dividing the neighboring water droplets are forced out of the way and nearby water droplets are able to coalesce.

At the regions of spontaneous jumping in absorbance there may exist rapid merging of water droplets with one another. In other words, the pockets of water increase in size (due to the polymer excreting water) to a point in which they will spontaneously coalesce (*Figure 3.24*). At concentrations in Region II, during this rapid coalescence the water rich phase remains as the dispersed phase while the protein rich phase remains as the continuous phase. Therefore, these changes should be reversible and upon cooling the sample should return to its original state. This behavior was observed after each test performed in Region II. The samples began as uniform solutions as seen in *Figure 3.22 B* and after returning to room temperature the solutions returned to this same uniform state.

In *Figure 3.24 A–C* is the slow gradual growth of the dispersed water rich droplets in the protein rich continuous phase in the region to the left of the dashed line in *Figure 3.24 F*. On the right hand side of the dashed line is where *D* and *E* lie in which the separately dispersed water droplets rapidly coalesce producing the spontaneous increase in absorbance.

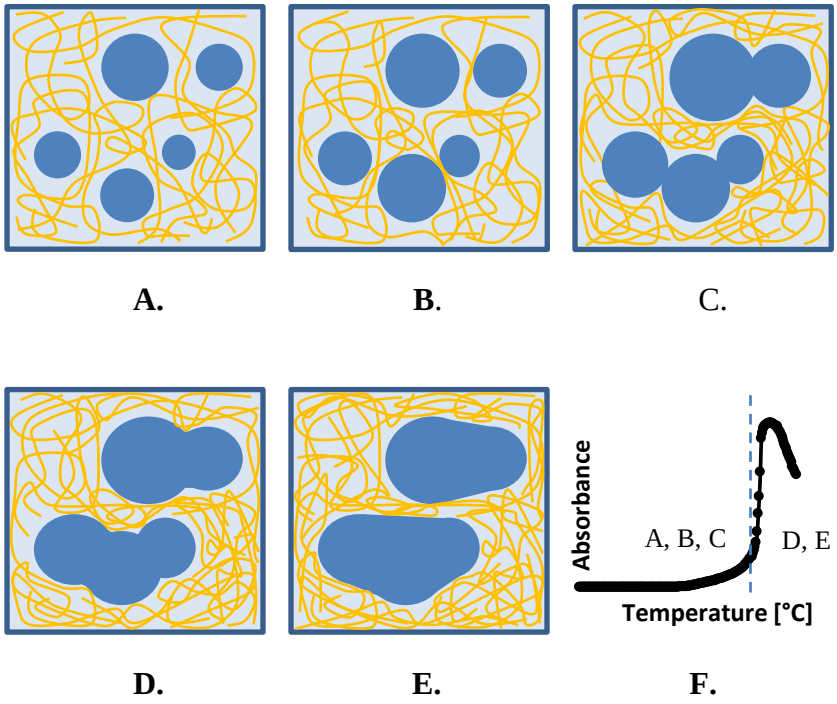

Figure 3.24: Transition from small dispersed water rich droplets to larger droplets due to excretion of water from the polymer with an increase in temperature. At the spontaneous T_t, at the point of rapid increase in absorbance, the water droplets rapidly coalesce. Represented by *A* through *C* is the slow gradual growth of the water droplets during the toe region to the left of the dashed lines in *F*. Represented in *D* and *E* is the rapid coalescing of neighboring water droplets in the region to the right of the dashed line in *F*.

Meyer and Chilkoti developed a model to predict the transition temperature of solutions of elastin-like polypeptides [44] on the basis of the phase diagram originally presented by Urry. The data gathered for the transition temperature of $(GVGVP)_{40}$ was analyzed and experimental results were compared to previously reported ELP systems. It was shown that at low concentrations ELP's transition temperatures show a linear dependency (*Figure 3.25*) on the logarithm of concentration [51].

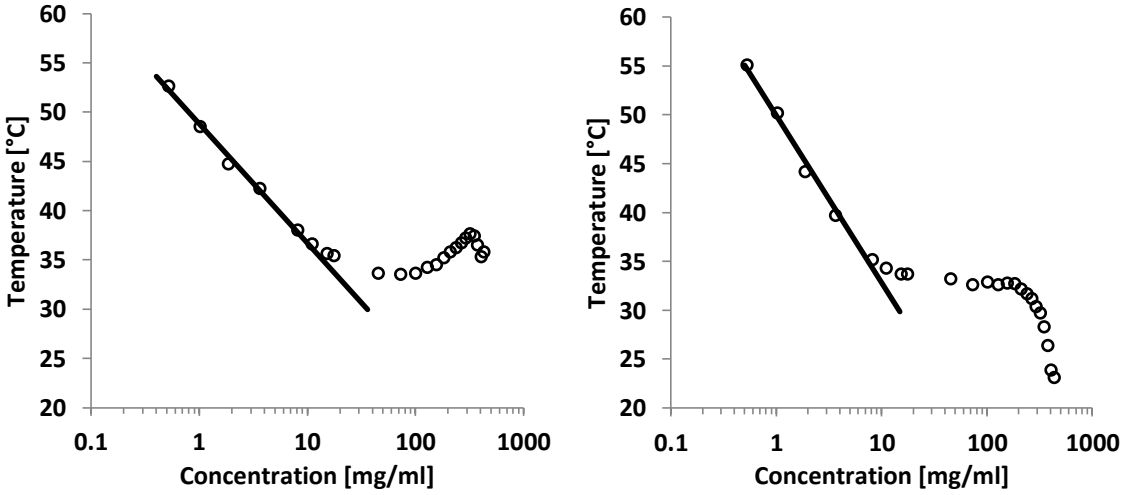

Figure 3.25: Linear relationship of T_t versus logarithm of concentration. Solid line represents the linearity observed at low concentrations on a T_t versus log concentration scale. Fit using both tangent line method (left) and modified tangent line method (right).

Using the model proposed by Meyer and Chilkoti, it is observed that the experimental data gathered in this study fits the model at low concentrations. The solid lines shown in *Figure 3.25* above represent the fit of the model for T_t versus the log of concentration. The temperature at which the line stops, approximately 30 °C, is the theoretical critical temperature at which the system transitions from dilute to semi-dilute as based on the work performed by Ghoorchian *et al* [51] adjusting for trace salt

conditions. An observation from the data at high concentrations shows a significant deviation from linearity in the plot shown above. At approximately 11 mg/ml, for the fits using both the tangent line and modified tangent line method, the transition temperatures observed no longer follow the linearity seen at low concentrations which is in agreement with work from Ghoorchian *et al* [51]. The concentration at which deviation occurs for both methods of determining T_t are nearly identical. The reason for this deviation is not certain, however it has been suggested that the deviation is due to the chain end effects [51]. The chain end effects may reduce the stabilizing effect of chain association thus, increasing the T_t.

Having an understanding of the behavior of this protein based polymer, the rheology data collected and explained in section *3.1* can be correlated to the phase transitioning analysis described in this section. Sadiku-Agboola *et al* discuss the rheological properties of polymers with a focus on two-phase systems [54]. The authors discuss how rheological properties of two-phase systems can depend on rheological behavior of the components and also the size, size distribution, and shape of discrete phase droplets dispersed in a continuous phase. The rheological properties of the multiphase systems can be strongly influenced by the morphology, which depends on the thermodynamic interactions [54]. Therefore, rheological properties can be useful in relating morphology of the phase-separated state of polymer systems [56].

Figure 3.26 shows the absorbance versus temperature graph for the 427 mg/ml sample. Examining the absorbance curve and analyzing using the tangent line method it was determined that the T_t is 36.0 °C. During the toe region of the absorbance versus temperature curve the changes in the system are subtle. It is at the large increase in

absorbance that the system has the most significant and spontaneous changes. For the system described in *Figure 3.8* and *Figure 3.9* there exists a distinct change in curvature when performing the effects of temperature analysis on a 427 mg/ml sample of $(GVGVP)_{40}$.When examining the rheological data gathered, it is expected that the most significant changes would be observed near the spontaneous coalescing of the water droplets at the sudden increase in absorbance.

Examining *Figure 3.9,* it is between 35 and 40 °C that there exists the change in curvature as described previously. The system shows systematic decreasing behavior prior to exceeding 35 °C. This behavior then deviates into a new behavior at temperatures greater than the proteins T_t. It is believed that this correlates directly with the rapid coalescing of the water droplets which happens at 36 °C. At this high concentration, the water droplets remain small because the polymer is viscous enough to prevent large scale movement of these droplets compared to lower concentrations. Therefore, at low temperatures below T_t, it may be much more difficult for polymer chains to be mobile. Exceeding the transition temperature the chains become more mobile, resulting in deviation in the rheological data.

To further show the dependence of the coalescence *Figure 3.27* shows the loss modulus with respect to temperature at angular frequencies of 50 to 500 rad/s. It is observed that for all frequencies from temperatures of 20 to 35 °C the log of the loss modulus decreases linearly with temperature. Upon exceeding temperatures of 35 °C (above T_t) the loss modulus exhibit significant deviation from the linear trend observed at lower temperatures thus further showing the dependence of the rapid coalescing of the water rich droplets.

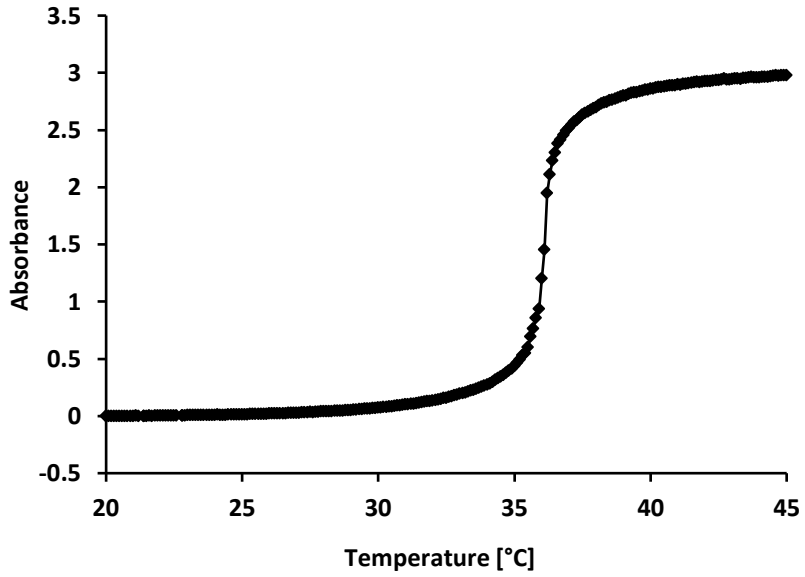

Figure 3.26: Absorbance versus temperature curve for $(GVGVP)_{40}$ at 427 mg/ml.

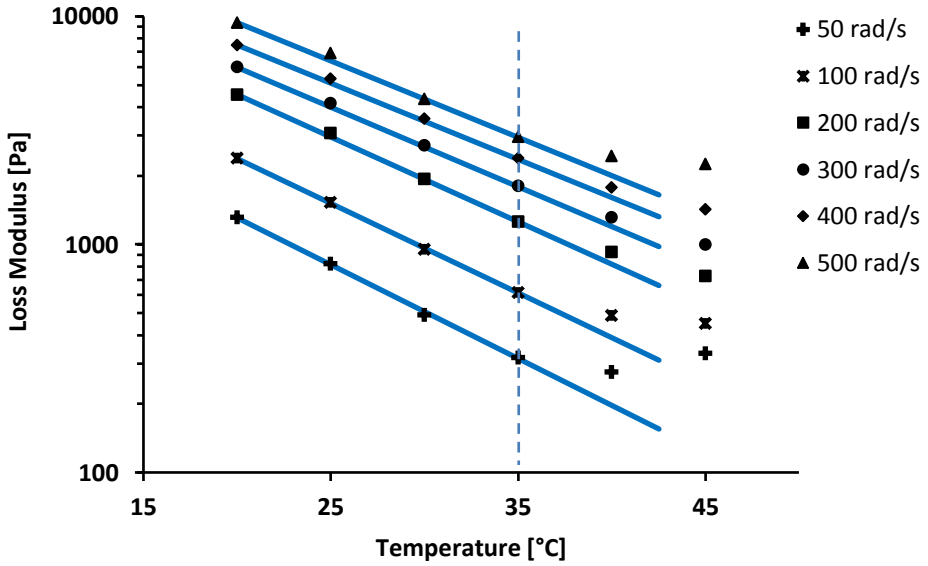

Figure 3.27: Loss modulus versus temperature at various frequencies for $(GVGVP)_{40}$ at 427 mg/ml.

CHAPTER IV

CONCLUSIONS

The elastin-like polypeptides $(GVGVP)_{40}$ and $(GVGVP)_{40}$-foldon were expressed and purified. Samples were made that consisted of high concentrations of protein. Many different types of tests were performed at these high concentrations to further understand these systems at such concentrations. Several tests were performed to determine the rheological properties of the protein coacervates. Using a combination of several techniques to analyze the UV-Visible spectrophotometer data, several phase diagrams were constructed to show the dependence of protein concentration on the transition temperature from a single phase to a multiple phase system.

We were able to determine that both the linear are trimerized systems fit a power law model at high concentrations of protein. This allows for the prediction of viscosity based on the protein concentration and shows the significance of the effects of increasing

concentrations on the system. There also exists a decreasing impact of concentration with increasing shear rates. Also, at low protein concentrations and trace salt conditions, the ELP follows the model which predicts the transition temperature with respect to concentration.

There exists a relationship between the rheological data collected and the phase transition behavior of these protein based polymers. When examining the phase diagrams constructed a common trend is observed in which a peak absorbance is observed at 322 mg/ml. Above this concentration the transition temperatures showed a change in which a decrease in T_t was observed. This behavior is not common to phase diagrams. This suggests that the method used in analyzing the transition temperature may not be the most ideal method, particularly for high protein concentrations.

Analysis of transition temperature should be examined using other analytical techniques (possibly NMR, calorimetry, or microwave techniques) to gather more information about the changes at high protein concentrations. It is suggested that future work be done using other analytical techniques in collaboration with the data gathered from the UV-Visible spectrophotometer to obtain a much better understanding of the phase transitioning behavior (especially in the region on the phase diagrams between the modified tangent line method and the tangent line method). Complimentary data could help better explain the change in phase transitioning behavior observed at high concentrations of elastin-like polypeptides. In doing so a more accurate and appropriate phase diagram may be constructed.

BIBLIOGRAPHY

[1] Cabello-Rodriguez J.C., Prieto, S. "Biofunctional Design of Elastin-like Polymers for Advanced Applications in Nanobiotechnology." *Journal of Biomaterial Science Polymer Edition*, 18, (**2006**), 269.

[2] Chow, D., Lim, D.W. "Peptide-based Biopolymers in Biomedicine and Biotechnology." *Materials Science and Engineering*, 62, (**2008**), 155.

[3] Circulis, J.T., Keeley, F.W. "Viscoelastic Properties of Gelation of an Elastin-like Polypeptide." *The Society of Rheology*, 53, (**2009**), 1215.

[4] Ghoorchian, A., Cole, J.T., Holland, N.B. "Thermoreversible Micelle Formation using a Three-Armed Star Elastin-like Polypeptide." *Macromolecules*, 43, (**2010**), 4340.

[5] Manz, A., Pamme, N., Iossifides, D. (**2004**, May), http://www.worldscibooks.com/chemistry/P297.html.

[6] Urry, D.W. "Entropic Processes in Protein Mechanisms. I. Elastic Structure due to an Inverse Temperature Transition and Elasticity due to Internal Chain Dynamics." *Journal of Protein Chemistry*, 7, (**1988**), 1.

[7] Urry, D.W., Trapane, T.L. "Phase-Structure Transitions of the Elastin Polypentapeptide-Water System within the Framework of Composition-Temperature Studies." *Biopolymers*, 24, (**1985**), 2356.

[8] Urry, D.W. “Physical Chemistry of Biological Free Energy Transduction as Demonstrated by Elastic Protein-Based Polymers.” *Journal of Physical Chemistry*, 101, (**1997**), 1128.

[9] Chilkoti, A., Christensen, T., MacKay, J.A. “Stimulus Responsive Elastin Biopolymers: Applications in Medicine and Biotechnology.” *Current Opinion in Chemical Biology*, 10, (**2006**), 657.

[10] Liu, W., Dreher, M.R., Furgeson, D.Y., Peixoto, K.V., Yaun, H., Zalutsky, M.R., Chilkoti, A. “Tumor Accumulation, Degradation and Pharmacokinetics of Elastin-like Polypeptides in Nude Mice.” *Journal of Controlled Release*, 116.2, (**2006**), 170.

[11] Paiva, L.R., Martins, M.L. “A Multiscale Model to Evaluate the Efficacy of Anticancer Therapies Based on Chimeric Polypeptide Nanoparticles.” *Applied Physics Letters*, 98.5, (**2011**), 53703.

[12] Chow, D., Nunalee, M., Lim, D.W., Simnick, A.J., Chilkoti, A. “Peptide-based Biopolymers in Biomedicine and Biotechnology.” *Materials Science and Engineering R*, 62.4, (**2008**), 125.

[13] Urry, D.W., Parker, T.M., Reid, M.C., Gowda, D.C. “Biocompatibility of the Bioelastic Materials, poly(GVGVP) and its Gamma-Irradiation Cross-Linked Matrix: Summary of Generic Biological Test Results.” *Journal of Bioactive and Compatible Polymers*, 6, (**1991**), 263.

[14] Urry, D.W., Pattanaik, A., Xu, J., Woods, T.C., McPherson, D.T., Parker, T.M. "Elastic Protein-Based Polymers in Soft Tissue Augmentation and Generation." *Journal of Biomaterials Science, Polymer Edition*, 9.10, (**1998**), 1015.

[15] Christiansen M., Matson, M., Brazg, R., Georgopoulos, L., Arnold, W., Kramer, W., Shi, L., Strange, P. "Weekly Subcutaneous Doses of PB1023 a Novel GLP-1 Analogue Reduce Glucose Exposure Dose Dependently." Phasebio.com/wp-content/uploads/2013/12/PosterPresentation-ADA-FINAL-6JUN2012-V1_Blackout-Version-17Jun20131.pdf., (**2014**, March).

[16] MacEwan, S.R., Chilkoti, A. "Applications of Elastin-like Polypeptides in Drug Delivery." *Journal of Controlled Release*, 190, (**2014**), 314.

[17] Hollister, S.J. "Scaffold Design and Manufacturing: From Concept to Clinic." *Advanced Materials*, 21.32, (**2009**), 3330.

[18] Nettles, D.L., Chilkoti, A., Setton, L.A. "Applications of Elastin-like Polypeptides in Tissue Engineering." *Advanced Drug Delivery Reviews*, 62.15, (**2010**), 1479.

[19] Meyer, D.E., Chilkoti, A. "Purification of Recombinant Proteins by Fusion with Thermally Responsive Polypeptides. *Nature Biotechnology*, 17.11, (**1999**), 1112.

[20] Andrade, J.D. "Hydrogels for Medical and Related Applications." *American Chemical Society Symposium Series*, (**1976**), 31.

[21] Lim, D.W., Nettles, D.L., Setton, L.A., Chilkoti, A. "Rapid Cross-Linking of Elastin-like Polypeptides with (Hydroxymethyl)phosphines in Aqueous Solution." *Biomacromolecules*, 8, (**2007**), 1463.

[22] Reguera, J., Urry, D.W., Parker, T.M., McPherson, D.T., Rodriguez-Cabello, J.C. "Endothermic and Exothermic Components of an Inverse Temperature Transition for Hydrophobic Association by TMDSC." *Journal of Chemical Physical Letters*, 388, (**2004**), 127.

[23] Urry, D.W. "Free Energy Transduction in Polypeptides and Proteins Based on Inverse Transition Temperature Transitions." *Progress in Biophysics and Molecular Biology*, 57, (**1992**), 23.

[24] Reguera, J., Urry, D.W., Parker, T.M., McPherson, D.T., Rodriguez-Cabello, J.C. "Effect of NaCl on the Exothermic and Endothermic Components of the Inverse Temperature Transition of a Elastin-like Polymer." *Biomacromolecules*, 8, (**2007**), 354.

[25] Girotti, A., Reguera, J., Arias, F.J., Alonso, M., Testera, A.M., Rodriguez-Cabello, J.C. "Influence on the Molecular Weight on the Inverse Temperature Transition of a Model Genetically Engineered Elastin-like pH Responsive Polymer." *Macromolecules*, 37, (**2004**), 3400.

[26] MacKay, A.J., Callahan, D.J., FitzGerald, K.N., Chilkoti, A. "Quantitative Model of the Phase Behavior of Recombinant pH-Responsive Elastin-like Polypeptides." *Biomacromolecules*, 11.11, (**2010**), 2873.

[27] Reguera, J., Urry, D.W., Parker, T.M., McPherson, D.T., Rodriguez-Cabello, J.C. "Effect of NaCl on the Exothermic and Endothermic Components of the Inverse Temperature Transition of a Model Elastin-like polymer." *Biomacromolecules*, 8, (**2007**), 358.

[28] Rodriguez-Cabello, J.C., Reguera, J., Alonso, M., Parker, T.M., McPherson, D.T., Urry, D.W. "Endothermic and Exothermic Components of an Inverse Temperature Transition for Hydrophobic Association by TMDSC." *Chemical Physics Letters*, 388, (**2004**), 127.

[29] Yamaoka, T., Tamura, T., Seto, Y., Tada, T., Kunugi, S., Tirrell, D.A. "Mechanism for the Phase Transition of a Genetically Engineered Elastin Model Peptide $(VPCIC)_{40}$ in Aqueous Solution." *Biomacromolecules*, 4.6, (**2003**), 1680.

[30] Von Hippel, P.H., Wong, K.Y. "On the Conformational Stability of Globular Proteins. The Effects of Various Electrolytes and Nonelectrolytes on the Thermal Ribonuclease Transition." *Journal of Biological Chemistry*, 240.10, (**1965**), 3909.

[31] Meyer, D.E., Chilkoti, A. "Quantification of the Effects of Chain Length and Concentration of the Thermal Behavior of Elastin-like Polypeptides." *Biomacromolecules*, 5.3, (**2004**), 846.

[32] Urry, D.W. "Molecular Machines: How Motion and Other Functions of Living Organisms Can Result from Reversible Chemical Changes." *Angewandte Chemie International Edition*, 32, (**1993**), 819.

[33] Baldwin, R.L. "The Nature of Protein Folding Pathways: The Classical Versus the New View." *Journal of Biomolecular NMR*, 5, (**1995**), 103.

[34] Urry, D.W. "Entropic Elastic Processes in Protein Mechanisms. II. Simple (Passive) and Coupled (Active) Development of Elastic Forces." *Journal of Protein Chemistry*, 7.2, (**1988**), 81.

[35] Nicolini, C., Ravindra, R., Ludolph, B., Winter, R. “Characterization of the Temperature- and Pressure-Induced Inverse and Reentrant Transition of the Minimum Elastin-Like Polypeptide GVG(VPGVG) by DSC, PPC, CD, and FT-IR Spectroscopy.” *Biophysical Journal*, 86.3, (**2004**), 1385.

[36] Urry, D.W. “The Change in Gibbs Free Energy for Hydrophobic Association: Derivation and Evaluation by Means of Inverse Temperature Transitions.” *Chemical Physics Letters*, 399, (**2004**), 177.

[37] Sartor, M. “Dynamic Light Scattering to Determine the Radius of Small Beads in Brownian Motion in a Solution.” https://physics.ucsd.edu/neurophysics/courses/physics_173_273/dynamic_light_scattering_03.pdf

[38] Bochicchio, B., Pepe, A., Tamburro, A.M. “Investigating by CD the Molecular Mechanism of Elasticity of Elastomeric Proteins.” *Chirality*, 20.9, (**2008**), 985.

[39] Tamburro, A.M., Lorusso, M., Ibris, N., Pepe, A., Bochicchio, B. “Investigating by Circular Dichroism some Amyloidogenic Elastin-Derived Polypeptides.” *Chirality*, (**2010**), 22.1

[40] Sandberg, L.B., Gray, W.R., Franzblau, C. “Elastin and Elastic Tissue.” *Advances in Experimental Medicine and Biology*, 79, (**1978**), 116.

[41] “Rheology. Oscillatory Shear Measurements.” http://www.uio.no/studier/emner/matnat/kjemi/KJM3100/v07/undervisningsmateriale/Lecture%202.pdf.

[42] Macosko, C.W. “Rheology: Principles, Measurements, and Applications.” First edition, *Wiley-VCH*, (**1994**, October).

[43] Urry, D.W., McPherson, D.T., Xu, J. “Product Purification by Reversible Phase Transition Following Escheria Coli Expression of Genes Encoding up to 251 Repeats of the Elastomeric Pentapeptide GVGVP.” *Protein Expression and Purification*, 7, (**1996**), 57.

[44] Meyer, D.E., Chilkoti, A. “Genetically Encoded Synthesis of Protein-Based Polymers with Precisely Specified Molecular Weight and Sequence by Recursive Directional Ligation.” *Biomacromolecules*, 3, (**2002**), 357.

[45] Walsh, G. “Proteins Biochemistry and Biotechnology”. First edition. *Wiley* (**2002**).

[46] Sambrook, J., Fritsch, E.F., Maniatis, T. “Molecular Cloning: A Laboratory Manual, 2nd Edition.” Cold Spring Harbor Press NY, 18.47 (**1989**) http://www.lifetechnologies.com/us/en/home/life-science/protein-expression-and-analysis/protein-gel-electrophoresis/sds-page.html

[47] Krukau, A., Brovchenko, I., Geiger, A. “Temperature Induced Conformational Transition of a Model Elastin-like Peptide GVP(VPGVG) in Water.” *Biomacromolecules*, 8, **(2007),** 2202.

[48] Nath, N., Chilkoti, A. “Interfacial Phase Transition of an Environmentally Responsive Elastin Biopolymer Adsorbed on Functionalized Gold Nanoparticles Studied by Colloidal Surface Plasmon Resonance.” *Journal of the American Chemical Society*, 123, **(2001)**, 8197.

[49] Urry, D.W., Haynes, B., Harris, R.D. “Temperature Dependence of Length of Elastin and its Polypeptapeptide.” *Biochemical and Biophysical Research Communications*, 141, **(1986)**, 749.

[50] Phillies, G.D.J. “Hydrodynamic Scaling of Viscosity and Viscoelasticity of Polymer Solutions, Including Chain Architecture and Solvent Quality Effects.” *Macromolecules*, 28, **(1995)**, 8198.

[51] Ghoorchian, A., Holland, N.B. “Molecular Architecture Influences the Thermally Induced Aggregation Behavior of Elastin-like Polypeptides.” *Biomacromolecules*, 22, **(2011)**, 4022.

[52] Phillies, G.D.J. “Range of Validity of Hydrodynamic Scaling Model.” *Journal of Physical Chemistry*, 96, **(1992)**, 10061.

[53] Cirulis, J.T., Keeley, F.W., James, D.F. “Viscoelastic Properties and Gelation of an Elastin-like Polypeptide.” *Journal of Rheology*, 53, **(2009)**, 1215.

[54] Sadiku-Agboola, O., Sadiku, E.R., Adegbola, A.T., Biotidara, O.F. “Rheological Properties of Polymers: Stucture and Morphology of Molten Polymer Blends.” *Materials Science and Applications*, 2, **(2011)**, 30.

[55] Sunthar, P. “Polymer Rheology.” http://www.physics.iitm.ac.in/~compflu/Lect-notes/sunthar.pdf

[56] Jeon, H.S., Nakatani, A.I., Han, C.C., Colby, R.H. “Melt Rheology of Lower Critical Solution Temperature Polybutadiene/Polyisoprene Blends.” *Macromolecules*, 33, **(2000)**, 9732.